

# Recursive Feasibility and Deadlock Resolution in MPC-based Multi-robot Trajectory Generation

Yuda Chen, Meng Guo and Zhongkui Li, *Senior Member, IEEE*

**Abstract**—Collision-free trajectory generation within a shared workspace is fundamental for most multi-robot applications. However, despite of their versatility, many widely-used methods based on model predictive control (MPC) lack theoretical guarantees on the feasibility of underlying optimization. Furthermore, when applied in a distributed manner, deadlocks often occur where several robots block each other indefinitely without resolution. Towards this end, we propose a systematic method called infinite-horizon model predictive control with deadlock resolution (IMPC-DR). It can provably ensure recursive feasibility and effectively resolve deadlocks online in addition to the handling of input and model constraints. The method is based on formulating a convex optimization over the proposed modified buffered Voronoi cells in each planning horizon. Moreover, it is fully distributed and requires only local inter-robot communication. Comprehensive simulation and experiment studies are conducted over large-scale multi-robot systems. Significant improvements of both feasibility and success rate are shown, in comparison with other state-of-the-art methods and especially in crowded and high-speed scenarios.

**Index Terms**—Multi-robot systems, motion planning, MPC, deadlock resolution, feasibility guarantee.

## I. INTRODUCTION

**C**OLLISION-free trajectory generation is essential for multi-robot systems to perform their missions in a shared environment, such as cooperative inspection, search, rescue and transportation [1]. However, it becomes especially challenging when a large number of robots navigate at high speed in a crowded space as shown in Fig. 1. As summarized in [2], the commonly-seen multi-robot trajectory generation (MRTG) algorithms can be classified into roughly five categories: potential fields [3], [4], [5] that design virtual driving forces induced by artificial potentials, which however often suffer from the problem of being stuck at local minimums; geometric guidance [6], [7], [8], [9] such as reciprocal velocity obstacles (RVO) that analyze the geometric properties based on the position and velocity of the whole team, which mostly neglect the underlying kinodynamic constraints; conflicts resolution [10], [11], [12] that relies on designing heuristic rules to resolve potential collisions, which often lacks guarantees on the collision avoidance; learning-based methods [13], [14], [15], [16] such as reinforcement learning that rely heavily on accurate simulators and thus suffers from the sim-to-real gap, as well as poor generalization to domains different from the training data; and optimization-based methods [17], [18],

The authors are with the State Key Laboratory for Turbulence and Complex Systems, Department of Mechanics and Engineering Science, College of Engineering, Peking University, Beijing 100871, China. Corresponding author: Zhongkui Li, zhongkli@pku.edu.cn.

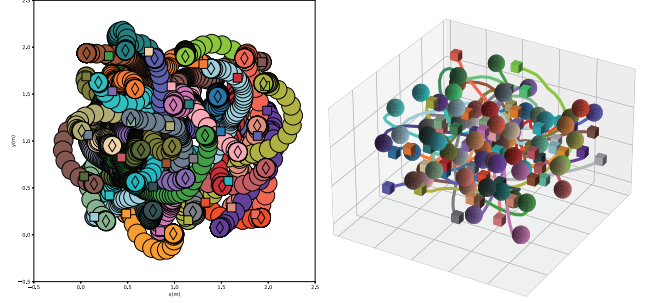


Fig. 1. High-speed navigation of 30 robots in a crowded 2D workspace (Left) and 60 robots in a crowded 3D workspace (Right).

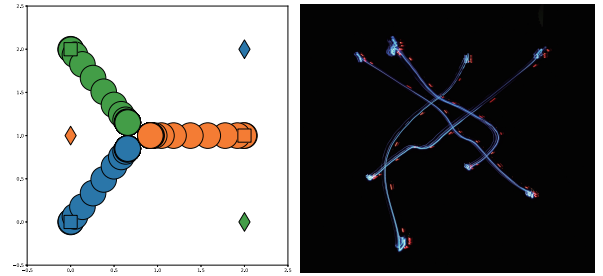


Fig. 2. **Left**: a typical case of deadlock due to symmetry, where filled cycles are robot trajectories and diamonds are their respective targets. **Right**: online deadlock resolution in the hardware experiment, where 4 robots try to transit to its antipodal position in a 3D cube.

[19], [20], [21] that have a better performance in versatility, extensibility and numerical stability. However, most of these aforementioned works lack in two critical aspects: feasibility guarantee and deadlock resolution. Consequently, collision-free trajectories are not always ensured to generate.

More specifically, optimization-based methods construct and solve various optimizations to achieve collision avoidance, such as the mixed integer quadratic programming in [18], sequential convex programming in [22], and model predictive control (MPC) in [23]. However, most of the aforementioned methods do not ensure explicitly feasibility of the underlying optimization. To address this problem, the work in [24] proposes to gradually add constraints to the sequence of convex programming when necessary. The authors in [25] further extend this idea to MPC and achieve simultaneous replanning by using the buffered Voronoi cell (BVC) [31]. Another work [26] introduces the notion of control barrier function, which can guarantee recursive collision-free trajectory. Nonetheless, it is overly conservative due to excessive breaking, and often suffers from deadlock. In addition, some other works in [27], [28] and [29] propose to tackle the feasibility problem by

TABLE I  
COMPARISON WITH RELATED WORK.

Reference	Distr. <sup>1</sup>	Meth. <sup>2</sup>	Online	Feasi. <sup>3</sup>	Dead.-free
[22], [27]	No	QP	No	No	Yes
[19]	No	NLP	No	No	Yes
[18]	Seq	MIP	Yes	No	Yes
[24]	Seq	QP	No	No	Yes
[23]	Seq	LP	Yes	No	Yes
[35]	Seq	NLP	Yes	No	Yes
[25], [31], [36]	Yes	QP	Yes	No	No
[26] <sup>4</sup>	Yes	QP	Yes	Yes	No
[34]	Yes	QP	Yes	No	Yes <sup>5</sup>
Ours	<b>Yes</b>	<b>SOCP</b>	<b>Yes</b>	<b>Yes</b>	<b>Yes</b>

<sup>1</sup> Distributed: 1) No: centralized, 2) Seq: sequentially, 3) Yes: distributed and simultaneously.

<sup>2</sup> Optimization method: 1) QP: quadratic program, 2) NLP: nonlinear program, 3) LP: linear program, 4) SOCP: second-order cone programming.

<sup>3</sup> Feasibility guarantee: 1) Yes: recursive feasibility, 2) No: no feasibility guarantee.

<sup>4</sup> See Section-VI of [26].

<sup>5</sup> Only for 3 robots.

gradually scaling the time step, which however requires centralized coordination. Recursive feasibility is ensured in [30], which however requires an extremely strict initial condition that may prohibit its usage for general trajectory generation. To summarize, recent works on optimization-based methods lack the formal guarantee on the feasibility of the underlying optimization process.

On the other hand, deadlock is another well-known issue in multi-robot trajectory generation. A deadlock happens when multiple robots are trapped by each other and cannot make any progress, as shown in Fig. 2. Typically, deadlock occurs due to the symmetry of the underlying system configuration, and more importantly the lack of a central coordinator. To resolve this issue, some methods [18], [22], [23] pre-define fixed priorities among the robots which only allows sequential adjustments of the trajectories, instead of simultaneous adjustments. Furthermore, the means of random perturbation is introduced in [31], [26] to break the equilibrium of deadlock. This however can lead to unpredictable behavior in practice as the magnitude of such perturbation is hard to determine. Thus the work in [32] extends this heuristic by adding a contingent trajectory to avoid potential collision caused by perturbation. However, the resulting trajectory does not take into account the kinematic feasibility. Furthermore, deadlocks can also be resolved by a high-level planner via re-planning [33], which however requires centralized coordination. The work in [34] formally addresses the deadlock problem but the proposed method is only applicable to no more than three robots. To summarize, as also pointed out in [31], there is *no existing algorithm* that can provably avoid deadlock in general cases without a central coordinator or global coordination.

To resolve the aforementioned issues, we propose a systematic trajectory generation algorithm (termed as IMPC-DR) that can guarantee recursive feasibility and resolve potential deadlocks online in a distributed manner. Its backbone is the proposed infinite-horizon model predictive control (IMPC). It ensures recursive feasibility by replacing the fixed goal

condition with a static terminal constraint in the underlying optimization. This additional static terminal constraint is inspired by the braking mechanism [26], [35], [38] and is commonly satisfied in practice such as a ground vehicle being immobile or a quadrotor hovering. Second, the traditional buffered Voronoi cells (BVC) in [31] is modified by introducing a velocity-dependent buffer width and a warning band into the IMPC. This novel modification is able to ensure collision avoidance not just at discrete time steps but for all time during navigation. Lastly, a necessary condition of multi-robot systems forming a deadlock is uncovered, which is equivalent to a force equilibrium. A deadlock detection mechanism is introduced to detect any potential deadlocks online and once detected, additional right-hand forces are computed in a distributed way to resolve these deadlocks.

As summarized in Table I, most existing optimization-based methods assume recursive feasibility without any guarantee, or relies on predefined robot priorities and sequential navigation for deadlock resolution. By contrast, our method IMPC-DR *for the first time* provably ensures recursive feasibility of MPC-based methods for MRTG and resolves potential deadlocks online without a central coordinator. The effectiveness of the proposed algorithms is verified by numerical simulations and hardware experiments. Compared with other state-of-the-art methods, our method shows a significant increase in both feasibility and success rate, especially for large-scale crowded and high-speed multi-robot systems.

The remaining part of this article is organized as follows. Section II describes the problem statement. The backbone of the our method IMPC is presented in Section III. The complete method IMPC-DR with online deadlock resolution is proposed in Section IV. Further details of the proposed algorithm are discussed in Section V. Section VI includes numerical simulations and hardware experiments. Conclusions and future work can be found in Section VII.

## II. PROBLEM STATEMENT

This section states formally the MPC-based multi-robot trajectory generation (MRTG) problem, and the exact notion of recursive feasibility and deadlock for MRTG.

### A. Robot Dynamics

Consider a team of  $N$  robots, where each robot  $i \in \mathcal{N} = \{1, 2, \dots, N\}$  is modeled as an unit mass in  $\mathbb{R}^d$ , and  $d = 2, 3$  is the dimension of the configuration space. Its state  $x^i = [p^{iT}, v^{iT}]^T$  includes position  $p^i$  and velocity  $v^i$ , and its acceleration  $u^i$  is the control input. Furthermore, its motion is approximated by the commonly-used second-order dynamics:

$$\dot{x}^i = \mathcal{A}x^i + \mathcal{B}u^i,$$

where  $\mathcal{A} = \begin{bmatrix} \mathbf{0}_d & \mathbf{I}_d \\ \mathbf{0}_d & \mathbf{0}_d \end{bmatrix}$ ,  $\mathcal{B} = \begin{bmatrix} \mathbf{0}_d \\ \mathbf{I}_d \end{bmatrix}$ . As often required in practice, both the robot velocity and acceleration are subjected to physical constraints. Specifically, it holds that  $\|\Theta_v v^i\|_2 \leq v_{\max}$  and  $\|\Theta_a u^i\|_2 \leq a_{\max}$ , where  $\Theta_v, \Theta_a$  are positive-definite matrices, and  $v_{\max}, a_{\max} > 0$  denote the maximum velocity and acceleration, respectively.

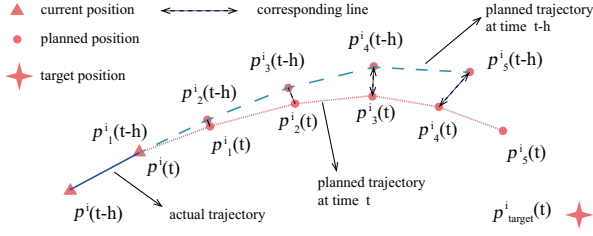


Fig. 3. Illustration of one replanning of the MPC-based MRTG with horizon length  $K = 5$ .

## B. Collision Avoidance

To avoid collision among the robots, the minimum distance allowed between any pair of robots is set to  $r_{\min} > 0$ . In other words, a collision happens when the distance between two robots  $i$  and  $j$  is lower than  $r_{\min}$ . Thus, collision is avoided for the whole system, if

$$\|p^i - p^j\|_2 \geq r_{\min} \quad (1)$$

holds, for any pair  $(i, j) \in \mathcal{N} \times \mathcal{N}$  and  $i \neq j$ .

## C. MPC-based MRTG

The general MRTG problem is to design control inputs  $u^i$  for each robot  $i \in \mathcal{N}$  such that it reaches the target position  $p^i_{\text{target}}$ , while avoiding collision with other robots at all time as required in (1).

As discussed in Section I, when solving MRTG problem by MPC-based methods, the robot trajectories are calculated by MPC at each time step and then executed in a receding horizon fashion. As illustrated in Fig. 3, only the first horizon of the planned trajectory is tracked by the lower-level controller. We assume that such controller exists and several candidates are mentioned in the sequel. More formally, the trajectory generation problem is always formulated and solved as a classic optimization problem. Similar to [23], consider a given time step  $h > 0$  and a finite planning horizon  $K$  (the choice of which will be discussed later). The MPC-based MRTG problem is stated as follows.

**Problem 1** (MPC-based MRTG). Design  $u^i_k(t)$  for robot  $i \in \mathcal{N}$  at time step  $t$  for each horizon  $k \in \{1, 2, \dots, K\}$  that solves the following optimization:

$$\min_{u^i_k(t), x^i_k(t)} \mathbf{C}(u^i_k(t), x^i_k(t)) \quad (2a)$$

$$\text{s.t.} \quad \|p^i_k(t) - p^j_k(t)\|_2 \geq r_{\min}, \quad \forall j \neq i, \forall k; \quad (2b)$$

$$p^i_K(t) = p^i_{\text{target}}; \quad (2c)$$

$$x^i_k(t) = \mathbf{A}x^i_{k-1}(t) + \mathbf{B}u^i_{k-1}(t), \quad \forall k; \quad (2d)$$

$$\|\Theta_a u^i_{k-1}(t)\|_2 \leq a_{\max}, \quad \forall k; \quad (2e)$$

$$\|\Theta_v v^i_k\|_2 \leq v_{\max}, \quad \forall k; \quad (2f)$$

where  $x^i_k(t) = [p^i_k(t)^T, v^i_k(t)^T]^T$  is the planned state in the  $k$ -th horizon for robot  $i$ ;  $p^i_k(t)$  is the planned position in horizon  $k$  of the planned trajectory  $\mathcal{P}^i(t) = \{p^i_1(t), p^i_2(t), \dots, p^i_K(t)\}$ ;  $p^i_0(t) = p^i(t)$  and  $v^i_0(t) = v^i(t)$  are current state at time step  $t$ ;  $\mathbf{C}(\cdot)$  is the cost function to be minimized;  $\mathbf{A}, \mathbf{B}$  represent

the discretized system matrices under the sampling time  $h$ , i.e.,

$$\mathbf{A} = \begin{bmatrix} \mathbf{I}_d & h\mathbf{I}_d \\ \mathbf{0}_d & \mathbf{I}_d \end{bmatrix}, \quad \mathbf{B} = \begin{bmatrix} \mathbf{0}_d \\ \mathbf{I}_d \end{bmatrix}. \quad (3)$$

It is worth noting that each robot can only dictate its own trajectory and *not* other robots'. However, a robot can exchange data with other robots via wireless communication. The objective is to solve the above problem collaboratively in a distributed manner without a central coordinator.

## D. Recursive Feasibility and Deadlock

As mentioned previously in Section I, there are two aspects of Problem 1 that are particularly challenging and of particular interest in this work: recursive feasibility and deadlock. Thus, we provide firstly their exact definitions below.

**Definition 1** (Recursive Feasibility). If the optimization in (2) is feasible at time step  $t-h$ , then the new optimization at time step  $t$  is also feasible.

**Definition 2** (Deadlock). Deadlock happens when all robots remain static indefinitely, but at least one robot has not reached its target position.

Recursive feasibility ensures safety of the resulting trajectories, namely no collision will happen. However, for certain configurations such as crowded scenarios, the robots may block each other and cannot make progress towards the targets, commonly known as deadlock [33]. Although no collision happens, this case still prohibits a successful navigation. In the subsequent sections, we will show how the main Problem 1 can be solved, with both recursive feasibility and deadlock resolution ensured.

## III. INFINITE HORIZON MODEL PREDICTIVE CONTROL

This section presents the backbone of the proposed solution to Problem 1, which is called the infinite-horizon model predictive control (IMPC). We show that via IMPC the recursive feasibility in Def. 1 is guaranteed.

### A. Choice of Horizon

Recursive feasibility of MPC is closely related to the horizon length  $K$  in Problem 1. Here, we first analyze this relation and discuss how to choose it.

Finite-horizon MPC is an approximation to infinite-horizon MPC in [37], where the horizon length  $K$  ought to be adequately long. Therefore, a goal condition in (2c) is enforced in Problem 1 for the target position. However, this constraint can be overly restrictive in many scenarios, especially when the problem is complex, rendering Problem 1 infeasible. As also proposed in [31], [25], the constraint in (2c) could be deleted and the deviation to the target is penalized in the cost function. However, this would indicate that the state at the terminal horizon, i.e.,  $x^i_{K-1}$ , does not have avoidance constraints since

<sup>1</sup>For the sake of simplicity, the time index will be omitted whenever ambiguity is not caused. For example,  $x^i_K(t)$  will be rewritten as  $x^i_K$ .

it has no corresponding position from the previous planned trajectory to form them, as shown in Fig. 3. Thus, an over-aggressive trajectory might be generated, causing infeasibility in the next optimization.

To address this problem, we add a terminal constraint to Problem 1 as follows:

$$x_K^i \in X_e, \text{ where } X_e = \{x \mid x = \mathbf{A}x + \mathbf{B}u, u \in U\}, \quad (4)$$

where  $X_e$  is a set of state which can have an available input to remain its state. For the system model in (2), the terminal constraint  $x_K^i \in X_e$  can be rewritten as  $v_K^i = \mathbf{0}_d$ . Furthermore, after adding a terminal static constraint in the optimization, we enforce that  $x_k^i = x_K^i, \forall k > K$ , which makes the actual planning horizon equal to infinity. Similarly, we enforce  $u_{k-1}^i = u_e$  for  $k > K$ , where  $u_e$  satisfies  $x_K^i = \mathbf{A}x_K^i + \mathbf{B}u_e$ .

**Remark 1.** This method is inspired by the braking mechanism in [26], [35], [38], in which safety is guaranteed by braking down. In addition, similar terminal constraints can be found in [35] which however does not consider recursive feasibility. It is worth noting that stationary is a common state in practice, i.e., a ground vehicle being immobile, a quadrotor hovering, or a fixed-wing aircraft flying at constant velocity. ■

### B. Reformulation of Collision Avoidance Constraint

In (2), the collision avoidance constraint is enforced explicitly by requiring the inter-robot distance to be more than  $r_{\min}$  at all time. However, the future states of other robots are not available at the current time. Thus, we propose to replace them with the *predetermined trajectory* of other robots. In other words, at each iteration, each robot will inform other robots its predetermined trajectory from the previous iteration.

**Definition 3** (Predetermined Trajectory (PT)). The predetermined trajectory for robot  $i$  at time  $t$  is defined as

$$\bar{\mathcal{P}}^i(t) = \{\bar{p}_1^i(t), \dots, \bar{p}_K^i(t)\},$$

where  $\bar{p}_k^i(t) = p_{k+1}^i(t-h)$  for  $k = 1, \dots, K$ . ■

Based on the predetermined trajectory, we use the spatial separation method to handle inter-robot collision avoidance. This method forming a separating hyperplane between different robots which restricts their corresponding motion space. In this article, inspired by [31], we define the following modified buffered Voronoi cell (MBVC) for robot  $i$  and  $j$  that  $j \neq i$ :

$$\mathcal{V}_k^{ij} = \left\{ p \in \mathbb{R}^d \mid \left( p - \frac{\bar{p}_k^i + \bar{p}_k^j}{2} \right)^T \frac{\bar{p}_k^i - \bar{p}_k^j}{\|\bar{p}_k^i - \bar{p}_k^j\|_2} \geq \frac{1}{2} r'_{\min} \right\}, \quad (5)$$

where  $\mathcal{V}_k^{ij}$  is the MBVC for robot  $i$  to  $j$  in horizon  $k$  for their given predetermined trajectory positions; and

$$r'_{\min} = \sqrt{r_{\min}^2 + h^2 v_{\max}^2} \quad (6)$$

is the extended buffer width. The term  $h^2 v_{\max}^2$  is vital to achieving collision avoidance between discretization points. Consequently, the collision avoidance constraints are decoupled and turn to  $p_k^i \in \mathcal{V}_k^{ij}, p_k^j \in \mathcal{V}_k^{ji}$ . Via simple

re-arrangements, the constraint in (5) can be rewritten as  $a_k^{ijT} p_k^i \geq b_k^{ij}, \forall j \neq i$ , where the coefficients are given by

$$a_k^{ij} = \frac{\bar{p}_k^i - \bar{p}_k^j}{\|\bar{p}_k^i - \bar{p}_k^j\|_2}, \quad b_k^{ij} = a_k^{ijT} \frac{\bar{p}_k^i + \bar{p}_k^j}{2} + \frac{r'_{\min}}{2}. \quad (7)$$

Note that the above reformulation retains the important property of collision avoidance as stated below.

**Proposition 1.** If  $a_k^{ijT} p_k^i \geq b_k^{ij}$  holds,  $\forall (i, j)$  and  $\forall k$ , then

$$\|p_k^i - p_k^j\|_2 \geq r'_{\min} \quad (8)$$

holds,  $\forall (i, j)$  and  $\forall k$ . And the planned trajectories are collision-free not only at the sampling points, such as  $p_{k-1}^i$  and  $p_k^i$ , but also at any points between them.

*Proof:* Refer to Appendix A for detailed derivations. ■

**Remark 2.** The MBVC defined in (5) is an extension of the buffered Voronoi cell (BVC) proposed in [31], which is defined as follows:

$$\bar{\mathcal{V}}^{ij} = \left\{ p \in \mathbb{R}^d \mid \left( p - \frac{p^i + p^j}{2} \right)^T \frac{p^i - p^j}{\|p^i - p^j\|_2} \geq \frac{1}{2} r_{\min}, \forall j \neq i \right\}.$$

The main difference is that the predetermined trajectory is introduced in MBVC while only the current robot position is used in BVC. The introduction of the predetermined trajectory and the extended buffer width dependent of the robot's maximum velocity in MBVC can ensure safety at all time instants as illustrated in Fig. 4, avoiding the potential scenario that collision may happen between two consecutive sampling points, as pointed out by [35]. ■

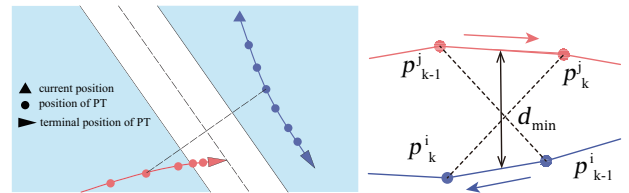


Fig. 4. **Left:** the split workspace in each horizon via MBVC. **Right:**  $d_{\min}$  is the minimum allowed distance from horizon  $k-1$  to horizon  $k$ .

### C. Choice of Cost Function

As mentioned earlier, the cost function in (2a) plays an important role in optimization. The proposed cost function for robot  $i$  is given by

$$C^i = \frac{1}{2} Q_{\text{tar}} \|p_K^i - p_{\text{target}}^i\|_2^2 + \frac{1}{2} \sum_{k=1}^{K-1} Q_{\text{adj}|k} \|p_{k+1}^i - p_k^i\|_2^2, \quad (9)$$

where  $Q_{\text{tar}}$  and  $Q_{\text{adj}|k} > 0, k = 1, 2, \dots, K-1$ , are the weighting parameters.

---

**Algorithm 1: IMPC for MRTG**


---

**Input** :  $p^i(t_0), p_{\text{target}}^i$   
**Output**:  $\mathcal{P}^i(t)$

```

1  $\bar{\mathcal{P}}^i(t_0) \leftarrow \text{InitialPT}(p^i(t_0))$ ;
2 while not all robots at target do
3   for  $i \in \mathcal{N}$  do
4      $\bar{\mathcal{P}}^j(t) \leftarrow \text{Communicate}(\bar{\mathcal{P}}^i(t))$ ;
5      $CONS^i \leftarrow \text{GetConstraints}(\bar{\mathcal{P}}^i(t), \bar{\mathcal{P}}^j(t))$ ;
6      $x^i(t) \leftarrow \text{GetCurrentState}$ ();
7      $\mathcal{P}^i(t) \leftarrow \text{ConvexProgram}(CONS^i, x^i(t))$ ;
8      $\bar{\mathcal{P}}^i(t+h) \leftarrow \text{GetPT}(\mathcal{P}^i(t))$ ;
9      $\text{ExecuteTrajectory}(\mathcal{P}^i(t))$ ;
10   $t \leftarrow t+h$ ;

```

---

#### D. Overall Algorithm

Based on the above discussions, the original optimization (2) is reformulated as the following convex optimization:

$$\min_{u^i, x^i} C^i \quad (10a)$$

$$\text{s.t. } a_k^{ijT} p_k^i \geq b_k^{ij}, \forall j \neq i, \forall k; \quad (10b)$$

$$v_K^i = \mathbf{0}_d; \quad (10c)$$

$$(2d) - (2f);$$

where the cost function in (10a), the collision avoidance constraints in (10b) and the terminal constraint in (10c) are as explained earlier; the rest of the constraints remain the same as in (2).

The complete algorithm is summarized in Alg. 1. First, the predetermined trajectory is initialized in Line 1 as  $\bar{\mathcal{P}}^i(t_0) = \{p^i(t_0), \dots, p^i(t_0)\}$ . Then, the robots start executing the main loop in parallel (Line 2). Each robot sends its predetermined trajectory to others and collects other's predetermined trajectory as  $\bar{\mathcal{P}}^j(t)$  (Line 4). Thereafter, each robot derives the collision avoidance constraints  $CONS^i$  (Line 5) and their current states  $x^i(t)$  (Line 6). Based on  $CONS^i$  and  $x^i(t)$ , the convex programming is solved (Line 7) and its solution, including the planned trajectory, is executed by the lower-level tracking controller (Line 9). Then, this procedure repeats itself until all the robots reach their target positions.

#### E. Recursive Feasibility Guarantee

Recursive feasibility, defined as in Def. 1, of the proposed method is ensured by the following theorem.

**Theorem 1.** *The convex optimization in (10) is recursively feasible under Alg. 1.*

*Proof:* To prove the recursive feasibility of the optimization in (10), we only need to show one feasible solution for the current convex optimization, given that the previous one is feasible. More specifically, a sufficient condition is that if  $x_k^i(t-h)$  and  $u_k^i(t-h)$  is a feasible solution to the optimization at time  $t-h$ , then  $x_k^i(t) = x_{k+1}^i(t-h)$  and

$u_k^i(t) = u_{k+1}^i(t-h)$  will satisfy all the constraints for the optimization at time  $t$ .

Firstly, it follows that

$$\begin{aligned}
 x_k^i(t) &= \mathbf{A}x_{k-1}^i(t) + \mathbf{B}u_{k-1}^i(t); \quad v_K^i(t) = \mathbf{0}_d; \\
 \|\Theta_a u_{k-1}^i(t)\|_2 &\leq a_{\max}; \quad \|\Theta_v v_k^i(t)\|_2 \leq v_{\max}.
 \end{aligned}$$

The above constraints hold since  $x_{k+1}^i(t-h) = x_k^i(t)$  and  $u_{k+1}^i(t-h) = u_k^i(t)$ , as the result of previous optimization, satisfy all above constraints. Thus, if the constraint in (10b) also holds, then all the constraints in (10) are satisfied. Substituting (7) into it yields

$$\|p_{k+1}^i(t-h) - p_{k+1}^j(t-h)\|_2 \geq r'_{\min}. \quad (11)$$

As a feasible solution at time  $t-h$ ,  $p_{k+1}^i(t-h)$  satisfies

$$a_{k+1}^{ijT}(t-h)p_{k+1}^i(t-h) \geq b_{k+1}^{ij}(t-h), \forall j \neq i, \forall k.$$

In combination with (8), the inequality in (11) holds, i.e., all the constraints in (10) are satisfied. Hence, the proof for recursive feasibility is completed. ■

**Remark 3.** Compared with [30], the constraints in (10) are less restrictive as we can easily find the following initially feasible condition: all robots are static and collision-free. ■

## IV. DEADLOCK RESOLUTION

The previous section proposes a solution to the MPC-MRTG problem, which ensures the recursive feasibility. In this section, we further improve this solution by adding a warning band to MBVC, and thus ensure that its solution is also deadlock-free.

#### A. Conditions for Deadlock

Based on Def. 2, when robot  $i$  is stuck at a deadlock, it stays at its current position and remains static. Namely, the planned position satisfies  $p^i(t) = p_1^i(t)$ , for  $t \geq t_{\text{deadlock}}$ , where  $t_{\text{deadlock}}$  is the starting time of deadlock. A deadlock can happen in the following two cases:

**Case 1:** for  $t \geq t_{\text{deadlock}}$ , there exist  $t$  and horizon  $k = 1, 2, \dots, K-1$  such that  $p_k^i(t) \neq p_{k+1}^i(t)$ , i.e., not all planned positions overlap;

**Case 2:** for  $t \geq t_{\text{deadlock}}$ ,  $p_k^i(t) = p_{k+1}^i(t)$ ,  $\forall k = 1, 2, \dots, K-1$ , i.e., all planned positions overlap.

In **Case 1**, the robots are blocked and remain static at horizon  $k = 1$ , but not all subsequent horizons, while in **Case 2**, the trajectory remains at one point, meaning that no further progress can be made unless the trajectory is updated.

For **Case 1**, since there exists a time  $t$  and horizon  $k$  such that  $p_k^i(t) \neq p_{k+1}^i(t)$  holds, the robots would not remain static indefinitely if its trajectory is not updated. Thus, when it occurs, robot  $i$  can remain at its current position until time  $t + (k+1)h$  when  $p_k^i(t) \neq p_{k+1}^i(t)$  holds. And its planned trajectory will be chosen as its predetermined trajectory. Consequently, the **Case 1** deadlock is resolved. In Section IV-C, it will be shown that this method can still maintain the recursive feasibility of IMPC.

As to **Case 2**, all horizon planned positions  $p_k^i$  overlap and are equal to  $p^i$ . The following lemma analyzes the condition for such deadlocks.

**Lemma 1** (Deadlock condition for **Case 2**). *Considering a set of robots  $\mathcal{N}_{case\ 2} \subseteq \mathcal{N}$  at **Case 2** deadlock, for each robot  $i \in \mathcal{N}_{case\ 2}$ , there exist  $j \in \mathcal{N}_{case\ 2}$  and  $\lambda_K^{ij}$  such that the following:*

$$Q_{tar} (p_{target}^i - p_K^i) + \sum_j \lambda_K^{ij} a_K^{ij} = 0 \quad (12)$$

holds, where  $a_K^{ij} = \frac{p^i - p^j}{\|p^i - p^j\|_2}$ . In addition, robot  $j$  is the robot that blocks robot  $i$ .

*Proof:* The proof is provided in Appendix B. ■

Based on Lemma 1, we define  $F_A^i = Q_{tar} (p_{target}^i - p_K^i)$  as the *attractive* force, which drives the planned position  $p_K^i$  to its target position. Similarly,  $F_R^{ij} = \lambda_K^{ij} a_K^{ij} \geq 0$  is defined as the *repulsive* force from robot  $j$  for robot  $i$  where  $a_K^{ij}$  and  $\lambda_K^{ij}$  are the direction and magnitude of this repulsive force, respectively. Thus, the deadlock condition (12) is a balance of these forces:

$$F_A^i + \sum_j F_R^{ij} = 0,$$

which is illustrated in Fig. 5. Note that the magnitude of the repulsive force, i.e.,  $\lambda_K^{ij}$  is only related to (12). Thus, its magnitude can be arbitrarily adjusted to make this equilibrium condition satisfied like robot 1 in Fig. 12, which is the idea behind the deadlock resolution in the subsequent subsection.

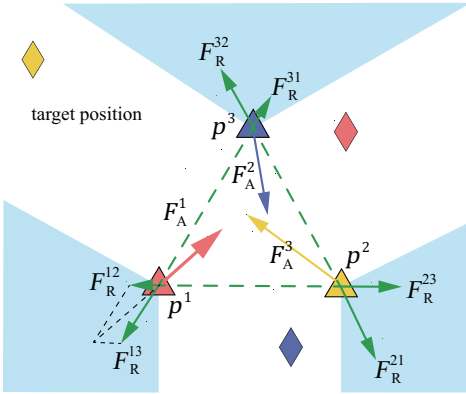


Fig. 5. Deadlock can be treated as a force equilibrium, where the attractive force from the target (in yellow, red, blue) and the repulsive forces from other robots (in green) are balanced. Take robot 1 as an example, the direction of repulsive force is determined by the relative position between its and other robots', the magnitude is adapted to balance the attractive force.

### B. Deadlock Resolution for Case 2

To ensure that the magnitude of repulsive forces are not arbitrary, we adopt the modified buffered Voronoi with warning band (MBVC-WB) at the terminal horizon  $K$ , as illustrated in Fig. 6.

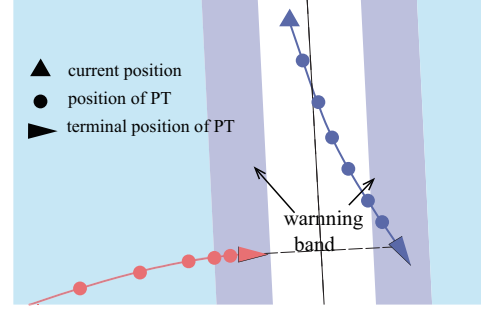


Fig. 6. Illustration of the MBVC-WB, where a warning band is additionally added.

**Definition 4** (MBVC-WB). The MBVC-WB for robot  $i \in \mathcal{N}$  and  $\forall j \neq i$  has a similar form as MBVC but it is only enforced at the terminal horizon  $K$  as follows:

$$\mathcal{V}_K^{ij} = \left\{ p \in \mathbb{R}^d \mid \left( p - \frac{\bar{p}_K^i + \bar{p}_K^j}{2} \right)^T \frac{\bar{p}_K^i - \bar{p}_K^j}{\|\bar{p}_K^i - \bar{p}_K^j\|_2} \geq \frac{r'_{\min}}{2} + w^{ij} \right\}$$

where  $w^{ij}$  is an additional variable added to the optimization. It is called the warning distance for robot  $i$  from  $j \neq i$ , which satisfies  $0 \leq w^{ij} \leq \epsilon$  and  $\epsilon$  is defined as the maximum width of warning band. ■

Based on the MBVC-WB above, the collision avoidance constraints can be written as  $a_K^{ijT} p_K^i \geq b_K^{ij} + w^{ij}, \forall j \neq i$ , where  $a_K^{ij}$  and  $b_K^{ij}$  are obtained from (7) as well. Meanwhile, an additional penalty term is added into the cost function:

$$C_w^i = \sum_{j \neq i} \rho_0 \left( \frac{w^{ij}}{\epsilon} - \ln w^{ij} \right), \quad (13)$$

where  $\rho_0 \in \mathbb{R}^+$  is a coefficient and  $w^{ij} > 0$ . Consequently, the objective function turns to

$$C^i = \frac{1}{2} Q_{tar} \|p_K^i - p_{target}^i\|_2^2 + \frac{1}{2} \sum_{k=1}^{K-1} Q_{adj|k} \|p_{k+1}^i - p_k^i\|_2^2 + \sum_{j \neq i} \rho_0 \left( \frac{w^{ij}}{\epsilon} - \ln w^{ij} \right).$$

Since the domain of  $w^{ij}$  is set to  $w^{ij} > 0$  in  $C_w^i$ , the constraints  $w^{ij} \geq 0$  is omitted.

To summarize, the convex optimization in (10) can be rewritten as follows:

$$\min_{u^i, x^i, w^{ij}} C^i \quad (14a)$$

$$\text{s.t. } a_k^{ijT} p_k^i \geq b_k^{ij}, \forall j \neq i, \forall k = 1, 2, \dots, K-1; \quad (14b)$$

$$a_K^{ijT} p_K^i \geq b_K^{ij} + w^{ij}, \forall j \neq i; \quad (14c)$$

$$w^{ij} \leq \epsilon; \quad (14d)$$

$$(10c), (2d) - (2f);$$

where (14a)-(14c) are different from (10).

Based on the new optimization, the condition in Lemma 1 turns to

$$Q_{tar} (p_{target}^i - p_K^i) + \sum_{j \in \mathcal{A}^i} a_K^{ij} \rho_0 \frac{\epsilon - w^{ij}}{\epsilon w^{ij}} = 0, \quad (15)$$

where  $\mathbb{A}^i \triangleq \{j | w^{ij} < \epsilon\}$  and  $w^{ji} = w^{ij}$  holds. The proof of equation (15) can be found in Appendix C. Similar to the analysis in Lemma 1,  $F_A^i = Q_{\text{tar}}(p_{\text{target}}^i - p_K^i)$  is the attractive force and  $F_R^{ij} = a_K^{ij} \rho_0 \frac{\epsilon - w^{ij}}{\epsilon w^{ij}}$  the repulsive force, where  $a_K^{ij}$  and  $\rho_0 \frac{\epsilon - w^{ij}}{\epsilon w^{ij}}$  are the direction and magnitude, respectively. The property in (15) can be rewritten as

$$F_A^i + \sum_{j \in \mathbb{A}^i} F_R^{ij} = 0. \quad (16)$$

**Remark 4.** The target positions chosen for the MRTG problem should be feasible. Namely, for any pair of robots  $i$  and  $j$ , their target positions should satisfy  $\|p_{\text{target}}^i - p_{\text{target}}^j\|_2 \geq r'_{\text{min}} + 2\epsilon$ , which implies no repulsive forces when they reach target positions. ■

**Proposition 2.** The necessary condition to form a deadlock is that the sum of all attracting force equal to zero, i.e.,

$$\sum_i F_A^i = \sum_i (p_{\text{target}}^i - p_K^i) = 0, \quad (17)$$

for robot  $i$  that is trapped in this deadlock.

*Proof:* Given (16), it holds that  $\sum_i (F_A^i + \sum_{j \in \mathbb{A}^i} F_R^{ij}) = 0$ . Since  $w^{ij} = w^{ji}$  and  $a_K^{ij} = -a_K^{ji}$ , clearly  $F_R^{ij} = -F_R^{ji}$  holds. By definition,  $j \in \mathbb{A}^i$  implies  $i \in \mathbb{A}^j$ . Then, it follows that  $\sum_i \sum_{j \in \mathbb{A}^i} F_R^{ij} = 0$  and thus (17) holds. ■

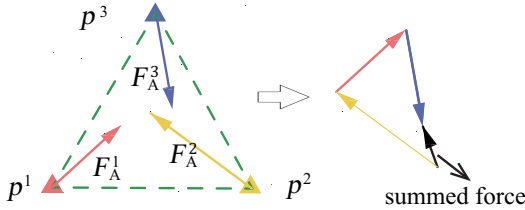


Fig. 7. The resulting force (black arrow) is non-zero, meaning that the force equilibrium in (16) does not hold.

Hence, due to this stricter condition, most deadlocks that might be caused by MBVC do not appear, as illustrated in Fig. 7. However, for some cases, the condition for **Case 2** deadlock might still hold. To deal with it, we adopt a detection-resolution method. Thus, an indicator to detect a potential **Case 2** deadlock is firstly defined in the following.

**Definition 5** (Terminal Overlap). A terminal overlap happens when  $p_K^i(t) = p_K^i(t-h)$ ,  $p_K^i(t) \neq p_{\text{target}}^i$ ,  $p_K^i(t) = p_{K-1}^i(t)$ , and  $p_{K-1}^i(t) = p_{K-2}^i(t)$  hold. ■

It is evident that if **Case 2** deadlock happens, the condition for a terminal overlap must hold. A terminal overlap induced by a deadlock has the same necessary condition as specified in (15). The proof is similar to the one in Appendix C.

**Remark 5.** Different from [26], the proposed algorithm can plan ahead in time by  $Kh$ . Thus, a potential **Case 2** deadlock, i.e., terminal overlap, can be detected before a deadlock happens in the future. ■

After detecting a terminal overlap, a right-hand driving rule is added to the navigation force as inspired by [39], i.e., the robot tends to avoid the robots on its left more than its right by

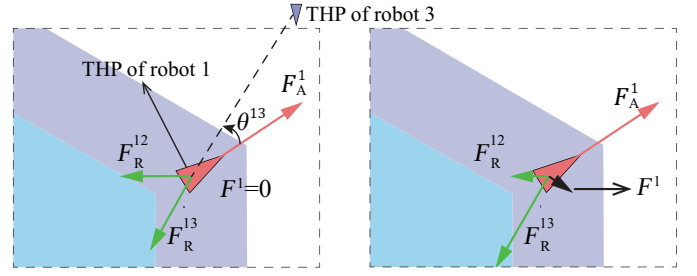


Fig. 8. Without right-hand force, the resulting force is zero (Left). The right-hand force makes the resulting force  $F^1$  non-zero, which might break the terminal overlap (Right). THP stands for terminal horizon position of predetermined trajectory.

generating right-hand forces. More specifically, if a terminal overlap is detected, replace  $\rho_0$  in (15) by  $\rho^{ij} = \rho_0 e^{(\eta \sin \theta^{ij})}$ , where  $\theta^{ij}$  is defined as the angular between the projection in  $x-y$  plane of line terminal predetermined trajectory position of robot  $i$  to its target position and the terminal predetermined trajectory position of robot  $j$ , as illustrated in Fig. 8;  $\eta > 0$  is a coefficient which can adjust the magnitude of right-hand force. As a result, the repulsive force from robot  $j$  to  $i$  is changed and the condition for the current terminal overlap does not hold anymore.

However, a new terminal overlap might happen again even after introducing the right-hand force. When a new terminal overlap is detected, then  $\eta$  is changed incrementally by

$$\begin{aligned} \eta^i(t) &= \eta^i(t-h) + \Delta\eta, \\ \rho^{ij} &= \rho_0 e^{(\eta^i(t) \sin \theta^{ij})}, \end{aligned} \quad (18)$$

where  $\Delta\eta > 0$  is a design parameter and  $\eta^i(t_0) = \eta_0$ , where  $\eta_0$  is a coefficient determining the initial magnitude of the right-hand force. Namely, the right-hand force is increased until the deadlock is resolved radically. Afterwards,  $\eta^i(t)$  is restored to  $\eta_0$  if  $w^{ij} = 0$  holds for  $j \neq i$ , i.e., its warning band have no contact with all others'.

### C. The Complete Algorithm: IMPC-DR

The complete method that incorporates the infinite-horizon model predictive control and the deadlock resolution (called IMPC-DR) is summarized in Alg. 2 with sub-functions defined in Alg. 4 and 3.

To begin with, several key boolean variables need to be introduced. More specifically,  $b_{\text{Case1}}^i$  is true when **Case 1** happens;  $b_{TO}^i$  returns true when a terminal overlap is detected;  $b_{TOA}^i$  is true when another terminal overlap is detected again.

The main loop in Alg. 2 runs as follows. Each robot checks if **Case 1** has happened. If so, the previously planned trajectory with receding horizon, i.e., predetermined trajectory is followed (Line 7) until some progress is made (Line 8). If a terminal overlap happens, it needs to check whether a terminal overlap happens again or not. If **Case 1** does not happen,  $\rho^{ij}$  is returned and Alg. 3 is followed (Line 11). Afterwards, the constraints for collision avoidance are derived (Line 12) as well as its current state (Line 13). Thereafter, the formulated optimization is solved in (10); see Line 14. Based on the results, boolean variables listed in Alg. 4 are computed

**Algorithm 2:** Complete IMPC-DR for MRTG

---

**Input :**  $p^i(t_0), p_{\text{target}}^i$   
**Output:**  $\mathcal{P}^i(t)$

- 1  $b_{\text{Case1}}^i, b_{TO}^i, b_{TOA}^i \leftarrow \text{False};$
- 2  $\bar{\mathcal{P}}^i(t_0) \leftarrow \text{InitialPT}(p^i(t_0));$
- 3 **while** not all agents at target **do**
- 4     **for** robot  $i$  **do**
- 5          $\bar{\mathcal{P}}^j(t) \leftarrow \text{Communicate}(\bar{\mathcal{P}}^i(t));$
- 6         **if**  $b_{\text{Case1}}^i$
- 7              $\mathcal{P}^i(t) \leftarrow \bar{\mathcal{P}}^i(t);$
- 8             **if**  $p_1^i(t) \neq p^i(t)$
- 9                  $b_{\text{Case1}}^i \leftarrow \text{False}$
- 10         **else**
- 11              $\rho^{ij} = \text{GetRho}(b_{TO}^i, b_{TOA}^i);$
- 12              $\text{CONS}^i \leftarrow$
- 13                  $\text{GetConstraints}(\bar{\mathcal{P}}^i(t), \bar{\mathcal{P}}^j(t));$
- 14                  $x^i(t) \leftarrow \text{GetCurrentState}();$
- 15                  $\mathcal{P}^i(t), w^{ij} \leftarrow$
- 16                      $\text{ConvexProgram}(\text{CONS}^i, x^i(t), \rho^{ij});$
- 17                  $b_{TO}^i, b_{TOA}^i, b_{\text{Case1}}^i \leftarrow$
- 18                      $\text{GetBoolean}(p^i(t), \mathcal{P}^i(t), w^{ij});$
- 19              $\bar{\mathcal{P}}^i(t+h) \leftarrow \text{GetPT}(\mathcal{P}^i(t));$
- 20              $\text{ExecuteTrajectory}(\mathcal{P}^i(t));$
- 21      $t \leftarrow t+h;$

---

**Algorithm 3:** GetRho( $\cdot$ )

---

**Input :**  $b_{TO}^i, b_{TOA}^i$   
**Output:**  $\rho^{ij}$

- 1 **if**  $b_{TO}^i$
- 2     **if**  $b_{TOA}^i$
- 3          $\eta^i(t) \leftarrow \eta^i(t-h) + \Delta\eta;$
- 4     **else**
- 5          $\eta^i(t) \leftarrow \eta^i(t-h);$
- 6      $\rho^{ij} \leftarrow \rho_0 e^{(\eta^i(t) \sin \theta^{ij})};$
- 7 **else**
- 8      $\rho^{ij} \leftarrow \rho_0, \eta^i(t) = \eta_0;$

---

in Line 15. Finally, the predetermined trajectory is obtained from the planned trajectory and sent to the feedback controller for execution in Line 17. The above procedure repeats itself until all robots have reached their target positions.

**Theorem 2.** *The complete algorithm IMPC-DR in Alg. 2 is recursive feasible and deadlock-free.*

*Proof:* (Sketch). To begin with, the proof for recursive feasibility is similar to the proof of Theorem 1. Namely, we need to show that all the constraints at the current time  $t$  are satisfied when both  $x_k^i(t) = x_{k+1}^i(t-h)$  and  $u_k^i(t) = u_{k+1}^i(t-h)$  hold. The updated trajectory in Line 7 of Alg. 2 can be treated as the solution to the optimization below:

$$\begin{aligned} & \min_{u_{k-1}^i, x_k^i, w^{ij}} \sum_k \|p_k^i - \bar{p}_k^i\|_2^2, \\ & \text{s.t.} \quad (14b) - (14d), (10c), (2d) - (2f), \end{aligned} \quad (19)$$

**Algorithm 4:** GetBoolean( $\cdot$ )

---

**Input :**  $p^i(t), \mathcal{P}^i(t), w^{ij}$   
**Output:**  $b_{TO}^i, b_{TOA}^i, b_{\text{Case1}}^i$

- 1 **if**  $p_{K-2}^i(t) = p_{K-1}^i(t) = p_K^i(t) = p_K^i(t-h) \neq p_{\text{target}}^i$
- 2     **if**  $b_{TO}^i$
- 3          $b_{TOA}^i \leftarrow \text{True}$
- 4     **else**
- 5          $b_{TOA}^i \leftarrow \text{False};$
- 6         **if**  $w^{ij} = \epsilon, \forall j \neq i$
- 7              $b_{TO}^i \leftarrow \text{False}$
- 8     **if**  $p^i(t) = p_1^i(t) \neq p_{\text{target}}^i$  and  $\exists k, p_k^i(t) \neq p_{k+1}^i(t)$
- 9      $b_{\text{Case1}}^i \leftarrow \text{True}$

---

which contains the same constraints as optimization (14). Then, if we can prove that the trajectory derived at time  $t-h$  is updated by either optimization (14) or (19), then  $\bar{\mathcal{P}}^i(t)$  is a feasible solution to both optimizations at time  $t$ .

When both  $x_k^i(t) = x_{k+1}^i(t-h)$  and  $u_k^i(t) = u_{k+1}^i(t-h)$  hold, constraints in (14b), (10c), (2d)-(2f) are satisfied as proven in Theorem 1. Then, towards the feasibility, not only the constraints (14c) and (14d) but also, for the demand of the domain of objective function (14a),  $w^{ij} > 0$  need to be satisfied. If  $a_K^{ijT}(t)p_{K+1}^i(t-h) > b_K^{ij}(t)$  holds for  $\forall j \neq i$ , and by choosing

$$w^{ij} = \min\{\epsilon, a_K^{ijT}(t)p_{K+1}^i(t-h) - b_K^{ij}(t)\},$$

then  $w^{ij} > 0$  holds as well as the constraints (14c) and (14d). Therefore, we only need to prove that

$$a_K^{ijT}(t)p_{K+1}^i(t-h) > b_K^{ij}(t), \quad (20)$$

holds for  $\forall j \neq i$ . Substituting  $a_K^{ij}(t)$  and  $b_K^{ij}(t)$  from (7) into (20) yields  $\|p_{K+1}^i(t-h) - p_{K+1}^j(t-h)\|_2 > r'_{\min}$ . Moreover, since  $p_{K+1}^i(t-h) = p_K^i(t-h)$  holds by definition, it yields

$$\|p_K^i(t-h) - p_K^j(t-h)\|_2 > r'_{\min}. \quad (21)$$

As a feasible solution at the previous time step,  $p_K^i(t-h)$  satisfies  $a_K^{ijT}(t-h)p_K^i(t-h) \geq b_K^{ij}(t-h) + w^{ij}(t-h)$ , for  $\forall j \neq i$ . Since  $w^{ij}(t-h) > 0$  holds, it follows that  $a_K^{ijT}(t-h)p_K^i(t-h) > b_K^{ij}(t-h)$ , which further implies that both the inequalities (21) and (20) hold. Thus, the recursive feasibility of (14) is retained.

Regarding the deadlock-free property, both the cases in Section IV-A should be discussed. The same analysis for **Case 1** still applies, while for **Case 2** it can be shown that a terminal overlap never happens. In Alg. 2, the potential equilibrium required by a terminal overlap is always prevented by the right-hand force in (18). This completes the proof. ■

## V. FURTHER DISCUSSIONS

In this section, we discuss some further issues related to the proposed method. Specifically, how the communication range among the robots is designed, and how the aforementioned parameters are chosen for different scenarios.



### A. Communication Range

Most related works [16], [18], [22], [23] require a fully-connected network, i.e., each robot is required to communicate with *all* other robots. This not only results in large communication overhead but also high computation burden. In this work, we propose a distance-based communication strategy that only requires local communication.

**Proposition 3** (Communication Range). *For any pair of robots  $(i, j)$ , no communication between them is required, if  $\|p^i - p^j\|_2 \geq 2v_{\max}Kh + r'_{\min} + 2\epsilon$  holds.*

*Proof:* A communication is not necessary, if it affects neither the recursive feasibility of the optimization nor the deadlock resolution.

Clearly, if  $\|p^i - p^j\|_2 \geq 2v_{\max}Kh + r'_{\min} + 2\epsilon$  holds, then  $\|p_k^i - p_k^j\|_2 \geq r'_{\min} + 2\epsilon$  holds for  $k = 1, 2, \dots, K$ . Hence, in the case of finite horizon  $K$ , no repulsive force between robots exists. Thus, no potential deadlock can be induced because of the interaction between them.

For robot  $i$ , if the predetermined trajectory from robot  $j$  is not received, the constraint (10b) is deleted. Therefore, the following *four* cases should be considered: (I) the constraint exists at both the previous time's and the current time's optimization; (II) the constraint only exists at the previous time; (III) the constraint exists at neither the previous time nor the current time; and (IV) the constraint only exists at the current time.

For Case (I), it is just the ordinary case which has been proved. For Case (II), as the property of recursive feasibility, the optimization without deleting this constraint is feasible. Then, deleting this constraint cannot make this optimization infeasible. For Case (III), obviously a constraint that is not introduced to convex programming will not affect the property of recursive feasibility. Case (IV), different from the other three cases, introduces a new constraint in the optimization at the current time. Firstly, since  $\|p^i - p^j\|_2 \geq 2v_{\max}Kh + r'_{\min} + 2\epsilon$  holds, it follows that  $\|p_k^i - p_k^j\|_2 \geq r'_{\min} + 2\epsilon, \forall k$ . This indicates that equation (11) in the proof of Theorem 1 and (21) in the proof of Theorem 2 hold automatically. Then, similar to these proofs, we can show that the predetermined trajectory is a feasible solution as well. ■

### B. Selection of Parameters in Algorithm 2

The parameters in Alg. 2 have significant influence on the performance of the overall algorithm. More specifically, the key parameters are the time step  $h$ , the horizon  $K$ , the width of warning band  $\epsilon$ , in addition to the penalty weights  $Q_{\text{tar}}$  and  $\rho_0$  in the cost function.

The time step  $h$  directly effects the buffer width of MBVC-WB as in (6). A larger  $h$  means a wider buffer, yielding a more conservative collision avoidance. On the other hand, a smaller  $h$  means a larger horizon  $K$  for the same planning time, leading to a larger optimization thus a higher complexity. Moreover,  $K$  should be larger than  $K_{\min}$  which is the minimum time that a robot needs to stop from any allowed velocity. Similarly, for a large maximum velocity  $v_{\max}$ , larger  $K$  and smaller  $h$  should be chosen to react faster and

plan further, which of course resulting in more computation complexity. A larger width of warning band  $\epsilon$  leads to a better deadlock-resolution performance, but in general a more sensitive reaction to deadlock, thereby longer time to accomplish the navigation task. The position penalty weight  $Q_{\text{tar}}$  and the warning penalty  $\rho_0$  directly influence the magnitude of the attractive and repulsive forces, respectively. A larger  $Q_{\text{tar}}$  results in a closer inter-robot distance and longer time while resolving potential deadlocks. Similarly, larger  $\eta_0$  and  $\Delta\eta$  means a larger right-hand force and thereby a better deadlock resolution, but may lead to a lower-quality trajectory.

## VI. SIMULATION AND EXPERIMENT

In this section, the proposed algorithm is validated via numerical simulations and hardware experiments of large-scale multi-robot systems. The algorithms are implemented in Python3, and publicly available at <https://github.com/PKU-MACDLab/IMPC-DR>. The convex optimizations are formulated by CVXPY [40] and solved by MOSEK [41]. The average time of replanning per one robot is around 0.06s. The numerical simulations include some typical scenarios such as swapping position, narrow passage and symmetry; and random transitions. For evaluation, our methods IMPC and IMPC-DR are compared with another three works: iSCP [24], DMPC [25] and BVC<sup>2</sup> [31]. The implementation of iSCP and DMPC is based on [42].

### A. Typical Scenarios

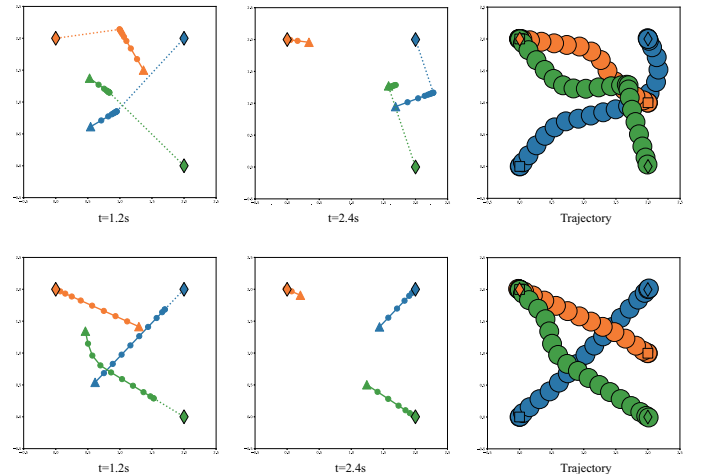


Fig. 9. The typical scenario of swapping positions. **Top:** The traditional BVC method may generate a zigzag motion as BVC is induced from the current position and adopted to all horizons. **Bottom:** By adopting MBVC to each horizon, our method can generate a much smoother trajectory.

To begin with, some typical scenarios in MRTG are considered. The maximum velocity  $v_{\max} = 1.0m/s$  and the maximum acceleration  $a_{\max} = 1.5m/s^2$ . In the simulation of typical scenarios, the time step  $h$  is chosen as 0.2s, the horizon length  $K = 10$ . The width of warning band  $\epsilon$  is chosen as 0.1m. In addition, we set position penalty weights  $Q_{\text{tar}} = 30.0$ ,  $\rho_0 = 2.0$  and  $\eta_0 = 2.0$ .

<sup>2</sup>In our simulation, the heuristically perturbation mechanism that handling deadlock is deleted as it often causes stability issue of the system.

TABLE II  
TIME OF RANDOM TRANSITIONS IN 3D

Method	the number of robots						
	2	4	6	8	10	12	14
IMPC-DR	2.35s	2.61s	3.13s	3.68s	4.12s	4.94s	5.51s
BVC [31]	2.86s	3.44s	3.93s	4.51s	5.24s	5.99s	6.80s

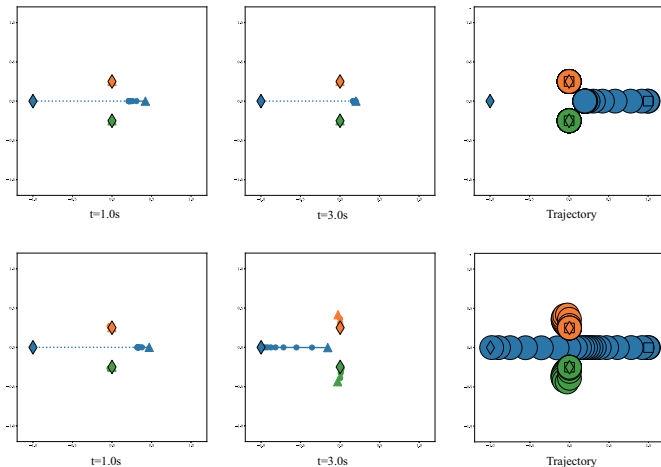


Fig. 10. The typical scenario of narrow passage where one robot passes through other two robots at target positions. **Top**: without the proposed warning band, the blue robot is blocked. **Bottom**: the introduction of the warning band to MBVC enables the blue robot to pass through the narrow gate.

1) *Swapping Position*: The first scenario is where the robots swap their positions, as shown in Fig. 9. In our method, MBVC is induced from the predetermined trajectory and adopted to each horizon instead of all horizons. Consequently, the planned trajectories of different robots can intersect, instead of being separated at all horizons in traditional BVC, see  $t = 1.2s$ . Thus, compared with BVC [31], our method has a shorter transition time as shown in Table II and smoother trajectories as depicted in Fig. 9.

2) *Narrow Passage*: The second typical scenario is where a robot needs to pass through another two robots who are already at their target positions. This scenario will show the necessity of adding the warning band of MBVC. As shown in Fig. 10, via MBVC-WB, this robot (blue) can squeeze out a way and, during squeezing, its slow movement compels others to get out of the way. The process of squeezing is inevitable since the force equilibrium (16) cannot hold at all in this case and, thus the deadlock can be avoided.

3) *Symmetry*: Lastly, symmetry is one of the common cases for deadlock. Thus, we consider such scenarios. In particular, four robots located in a  $2m \times 2m$  square transit to their antipodal positions. As shown in Fig. 11, robots approach the center point initially, and then, owing to the right-hand force, they change their direction to the right at around  $1.0s$ . Finally, after this right rotation, they escape this symmetry or, in other words, a potential deadlock at around  $3.0s$ . In comparison, without the deadlock resolution introduced in Section IV, **Case 2** deadlock happens, also shown in Fig. 11. The same phenomenon also appears in the 3D case as shown in Fig. 12,

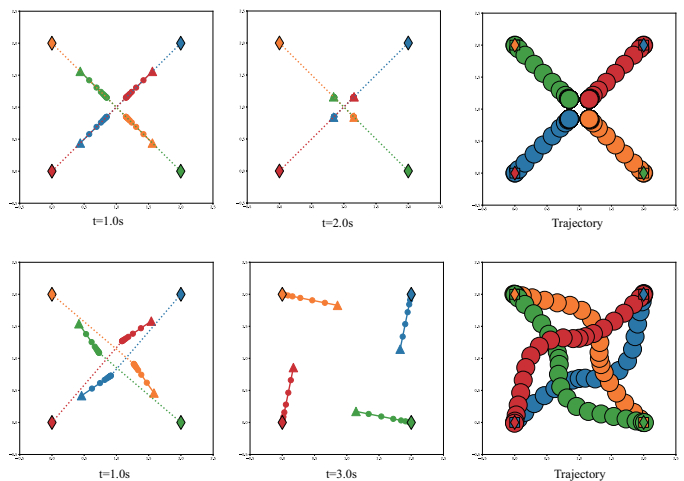


Fig. 11. **Top**: Without deadlock resolution, the robots are blocked by each other. **Bottom**: With the proposed right-hand forces, the robots can avoid deadlock.

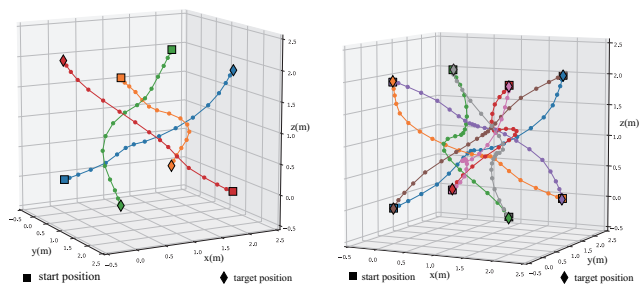


Fig. 12. Symmetric navigation to the antipodal corners in a cube by 4 robots (**Left**) and 8 robots (**Right**).

where the designed right-hand force drives the system away from the force equilibrium.

### B. Random Transitions

To systematically compare our method with other baselines, we consider the scenarios where the initial and target positions are randomly chosen, especially in crowded and high-speed 2D or 3D workspace. 100 tests are generated for each scenario. In each test, we determine it as success if all robots arrive at their target positions within a limited time and does not suffer from any infeasibility of optimization.

1) *Crowded 2D Workspace*: The 2D workspace is set to  $2m \times 2m$  and the number of robots ranges from 2 to 14. The safety diameter of a robot is chosen as  $0.3m$ . The maximum velocity, maximum acceleration, the warning band width and other parameters are selected the same as before. The only change is that the time step  $h = 0.15$  and the horizon length  $K = 12$ . The result is summarized in Table III and the process is shown in Fig. 13. It is clear that only IMPC and IMPC-DR do not suffer from infeasibility. Moreover, IMPC-DR can achieve almost 100% success rates in any density. Even for the highly crowded case of 14 robots, the success rate remains 87% for IMPC-DR, much higher than other baselines. It should be noted that the failed tests are caused by the time limitation instead of deadlock. Furthermore, it is worth noting that, after

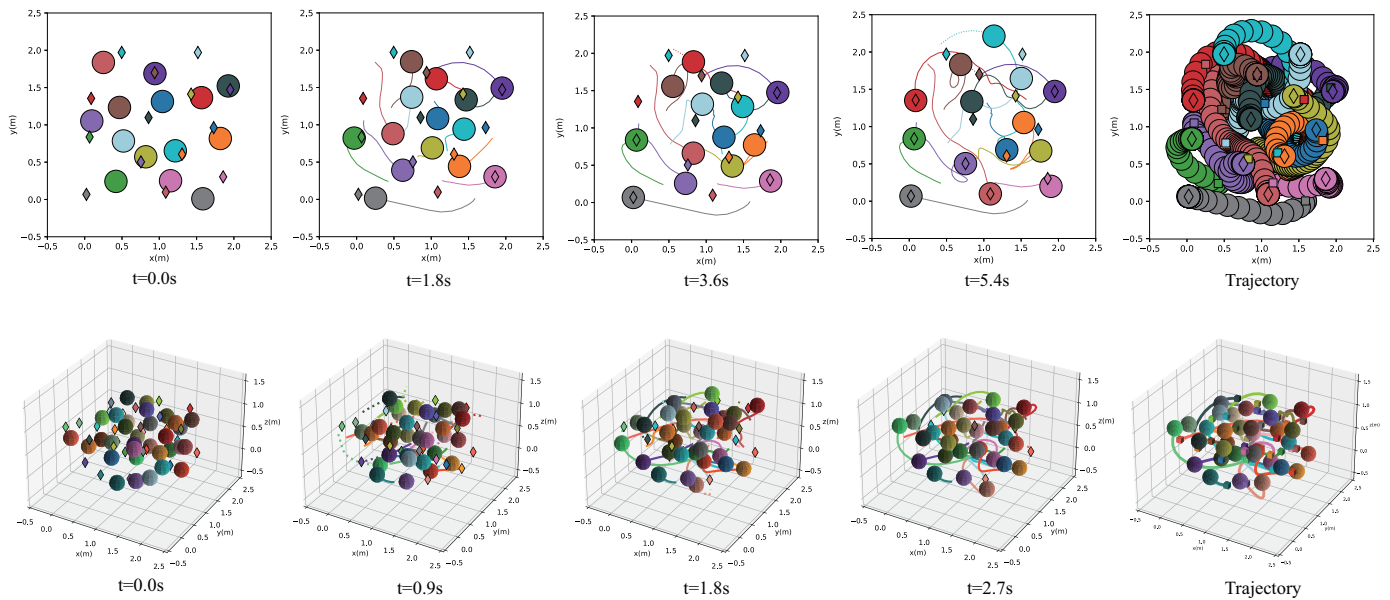


Fig. 13. Snapshots of the crowded navigation tasks via the proposed method in 2D by 14 robots (**Top**) and in 3D by 32 robots (**Bottom**). The actual trajectories are in solid lines while the predetermined trajectories are in dotted lines.

TABLE III  
RANDOM TRANSITIONS IN CROWDED 2D SCENARIOS

Metric	Method	the number of robots						
		2	4	6	8	10	12	14
Success	IMPC-DR	<b>100</b>	<b>100</b>	<b>100</b>	<b>100</b>	<b>100</b>	<b>99</b>	<b>87</b>
	IMPC	100	96	82	71	45	16	9
	BVC [31]	97	96	83	71	35	20	7
	iSCP [24]	100	99	94	81	58	39	12
	DMPC [25]	100	99	98	91	95	73	63
Infeas.	IMPC-DR	<b>0</b>	<b>0</b>	<b>0</b>	<b>0</b>	<b>0</b>	<b>0</b>	<b>0</b>
	IMPC	0	0	0	0	0	0	0
	BVC [31]	2	3	3	2	1	0	0
	iSCP [24]	0	1	6	19	20	61	88
	DMPC [25]	0	1	2	9	5	27	37

TABLE IV  
RANDOM TRANSITIONS IN CROWDED 3D SCENARIOS

Metric	Method	the number of robots						
		8	12	16	20	24	28	32
Success	IMPC-DR	<b>100</b>	<b>100</b>	<b>100</b>	<b>100</b>	<b>100</b>	<b>100</b>	<b>100</b>
	IMPC	100	100	100	100	99	93	90
	BVC [31]	100	100	100	99	99	98	86
	iSCP [24]	100	100	96	95	91	78	62
	DMPC [25]	100	94	85	74	66	62	46
Infeas	IMPC-DR	<b>0</b>	<b>0</b>	<b>0</b>	<b>0</b>	<b>0</b>	<b>0</b>	<b>0</b>
	IMPC	0	0	0	0	0	0	0
	BVC [31]	0	0	0	0	0	0	0
	iSCP [24]	0	0	4	5	9	22	38
	DMPC [25]	0	6	15	26	34	38	54

choosing  $\epsilon$  as  $0.1m$ , 14 robots are almost the *highest* capacity for this finite space. This illustrates that our method is capable of handling extremely crowded scenarios.

2) *Crowded 3D Workspace*: The 3D workspace is set to  $2m \times 2m \times 1m$ , where the number of robots ranges from 8 to 32. The robots share the same parameters as in the 2D case. The process is shown in Fig. 13. As summarized in Table IV, similar conclusions can be drawn as in the 2D case. Namely, IMPC and IMPC-DR do not suffer from infeasibility while only IMPC-DR achieves nearly 100% success rate for *any* number of robots. It is interesting to notice that deadlocks are less likely to appear in the 3D workspace than the 2D counterpart.

3) *High-Speed 2D and 3D Workspaces*: Last but not least, another key aspect is the high-speed scenario where online adaptation is essential for the successful navigation. In particular, the maximum velocity and acceleration are set to  $3m/s$  and  $2m/s^2$ , respectively; the workspace is extended to  $10m \times 10m$  and  $10m \times 10m \times 5m$  for 2D and 3D respectively. In this scenario, the safety diameter of all robots is set to  $1m$  and

the warning band width is extended to  $0.2m$ . As summarized in Table V and Table VI, the proposed method IMPC-DR can maintain the same performance in terms of feasibility and the 100% success rate. In contrast, the performance of other baselines such as BVC, iSCP and DMPC degraded significantly, due to mostly over-aggressive trajectories. This highlights the importance of our infinite horizon formulation and the added terminal constraint in (10c).

### C. Experiments

To further validate the proposed method, several experiments are performed on a nano quadrotor platform.

1) *Hardware Setup*: As shown in Fig. 14, the platform consists of several nano quadrotors, based on Bitcraze Crazyfile 2.1. They have  $9cm$  rotor-to-rotor and weight  $34g$ . Their states in the workspace are captured by OptiTrack, an indoor motion capture system, of which the update frequency is  $120Hz$ . This information is sent to the main control computer where the proposed trajectory generation algorithm is carried out for all quadrotors. The trajectory of quadrotor is fitted to a  $7_{th}$ -order

TABLE V  
RANDOM TRANSITION IN HIGH-SPEED 2D SCENARIOS

Metric	Method	the number of robots						
		2	4	6	8	10	12	14
Success	IMPC-DR	100	100	100	100	100	100	100
	IMPC	100	98	93	77	68	49	37
	BVC [31]	95	77	58	42	31	23	11
	iSCP [24]	93	57	32	6	6	0	0
	DMPC [25]	98	86	65	39	33	10	4
Infeas	IMPC-DR	0	0	0	0	0	0	0
	IMPC	0	0	0	0	0	0	0
	BVC [31]	5	23	41	52	54	63	70
	iSCP [24]	7	43	68	94	94	100	100
	DMPC [25]	2	14	35	61	67	90	96

TABLE VI  
RANDOM TRANSITIONS IN HIGH-SPEED 3D SCENARIOS

Metric	Method	the number of robots						
		8	12	16	20	24	28	32
Success	IMPC-DR	100	100	100	100	100	100	100
	IMPC	100	100	99	99	100	99	98
	BVC [31]	95	77	58	42	31	23	11
	iSCP [24]	49	14	5	1	0	0	0
	DMPC [25]	83	55	36	23	12	5	0
Infeas	IMPC-DR	0	0	0	0	0	0	0
	IMPC	0	0	0	0	0	0	0
	BVC [31]	5	23	42	58	69	77	89
	iSCP [24]	51	86	95	99	100	100	100
	DMPC [25]	17	45	64	77	88	95	100

polynomial and then sent to other quadrotors along with its state information via high-frequency radio. After receiving the position information, Kalman filter is used to estimate the current velocity and position. A feedback controller is used to track the updated trajectory based on the work in [43] which ensures high tracking accuracy.

Furthermore, to avoid the inter-quadrotor air turbulence, the minimum distance between quadrotors  $r_{\min}$  is chosen as  $0.3m$  and the width of warning band  $\epsilon$  is chosen as  $0.1m$ . The maximum velocity and acceleration of Crazyfile are set to  $1m/s$  and  $1m/s^2$ , respectively, to ensure safety. Lastly, the time step  $h$  is set to  $0.2s$  and the horizon length 15, to balance the control performance and the computation burden.

2) *Results*: Similar to the numerical simulations, three typical cases are considered in the hardware experiment: 4 robot antipodal transition in 2D and 3D, see Figs. 11 and 12, and narrow passage in Fig. 10. More specifically, Fig. 15(a) shows one navigation result of 4 robots to their antipodal positions in a square. Different from the simulations, the width of the square is smaller than  $1m$ . Similar results in 3D are shown in Fig. 15(b). Collision avoidance is also validated by plotting the relative distance between any pair of robots against the minimum distance  $0.38m$ . Fig. 15(c) is the result of the typical deadlock resolution, where the minimum distance is  $0.34m$ .

Generally speaking, the results of hardware experiments are consistent with the findings in numerical simulations. However, we notice that due to communication or computation

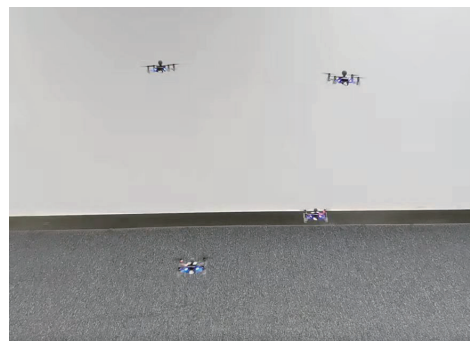
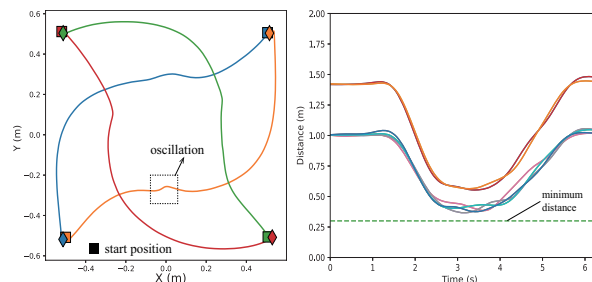
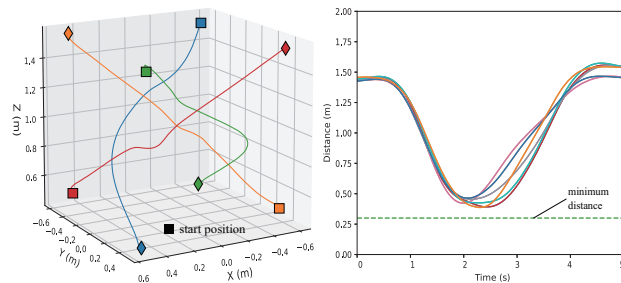


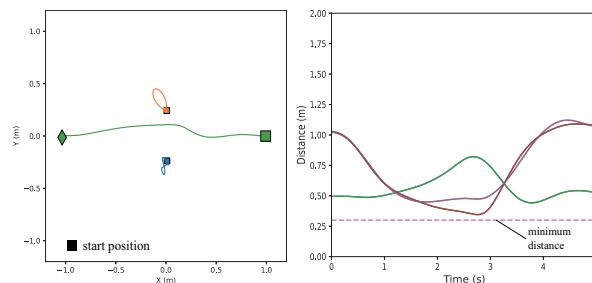
Fig. 14. Hardware platform consists of a team of Crazyflies nano quadrotors, a motion capture system, and a control computer.



(a) Four robots transit to their antipodal positions in a square. **Left**: Trajectory of robots. **Right**: Distance between robots.



(b) Four robots transit to their antipodal positions in a cube. **Left**: Trajectory of robots. **Right**: Distance between robots.



(c) A typical deadlock resolution demo. **Left**: Trajectories of robots. **Right**: Distance between robots.

Fig. 15. Hardware experiments of several scenarios, which can be compared with the numerical simulations in Section VI-A.

delays, execution of the computed trajectories is not exactly synchronized among the robots. For instance, as shown in Fig. 15(a), the robot in orange updates and executes its trajectory  $0.05s$  later than the robot in green, which is non-negligible compared with the updating frequency  $5Hz$ . Although some oscillations might appear, the overall navigation task remains

successful. It shows that our method is robust to asynchronous executions among the robots.

## VII. CONCLUSION

This work has proposed a novel and effective navigation algorithm called IMPC-DR for multi-robot systems. It provably ensures recursive feasibility of the underlying optimization, while resolving any potential deadlocks online. Compared with other state-of-the-art baselines, its advantages in crowded and high-speed scenarios are significant, as demonstrated both in simulations and hardware experiments. Future work includes the extension to obstacle-rich environments in combination with search-based planning methods.

### APPENDIX A PROOF OF PROPOSITION 1

To prove Proposition 1, we need the following lemma.

**Lemma 2.** *Consider two line segments in 2D: the line segment from  $p_1$  to  $p_2$  and the line segment from  $q_1$  to  $q_2$ , where  $p_1, p_2, q_1, q_2 \in \mathbb{R}^2$ . If*

$$\|r_1\|_2, \|r_2\|_2 \geq \sqrt{r_{\min}^2 + \frac{1}{4}\|l_2 - l_1\|_2^2} \quad (22)$$

is satisfied for  $r_1 = q_1 - p_1$ ,  $r_2 = q_2 - p_2$ ,  $l_1 = p_2 - p_1$  and  $l_2 = q_2 - q_1$ , then

$$\|p_1 + t(p_2 - p_1) - q_1 - t(q_2 - q_1)\|_2 \geq r_{\min} \quad (23)$$

holds,  $\forall t \in [0, 1]$ .

*Proof of Lemma 2:* It is trivial to show that the left-hand side of (23) is equivalent to

$$p_1 + t(p_2 - p_1) - q_1 - t(q_2 - q_1) = r_1 + t(r_2 - r_1).$$

Hence, it suffices to prove that

$$\|r_1 + t(r_2 - r_1)\|_2 \geq r_{\min}, \quad \forall t \in [0, 1].$$

Let us introduce a function  $F(t) = \|r_1 + t(r_2 - r_1)\|_2^2$ , where  $t \in [0, 1]$ . Moreover, set  $F(t_{\min}) = \min_{t \in [0, 1]} F(t)$ , where  $t_{\min} \in [0, 1]$  is the time instant where  $F(t)$  reaches its minimum.

Consider the following two cases: First, when  $r_1 = r_2$  holds, it follows that  $F(t) = r_1^T r_1 = \sqrt{r_{\min}^2 + \frac{1}{4}\|l_2 - l_1\|_2^2} \geq r_{\min}^2$ ; Second, when  $r_1 \neq r_2$  holds, we consider further the following three sub-cases: (i) if  $t_{\min} = 0$  holds, then  $F(0) = r_1^T r_1 \geq r_{\min}^2$ ; (ii) if  $t_{\min} = 1$  holds, then  $F(1) = r_2^T r_2 \geq r_{\min}^2$ ; (iii) if  $0 < t_{\min} < 1$  holds, the minimum of the quadratic function  $F(t)$  is given by

$$F(t_{\min}) = \frac{r_1^T r_1 r_2^T r_2 - r_1^T r_2 r_1^T r_2}{(r_2 - r_1)^T (r_2 - r_1)},$$

where  $t_{\min}$  is equal to

$$t_{\min} = \frac{r_1^T (r_2 - r_1)}{(r_2 - r_1)^T (r_2 - r_1)}. \quad (24)$$

To prove  $F(t_{\min}) \geq r_{\min}^2$ , it is equivalent to showing that

$$r_1^T r_1 r_2^T r_2 - r_1^T r_2 r_1^T r_2 \geq r_{\min}^2 (r_2 - r_1)^T (r_2 - r_1). \quad (25)$$

After simple calculations, (25) can be rewritten as

$$\begin{aligned} & (r_1^T r_1 - r_{\min}^2) (r_2^T r_2 - r_{\min}^2) \\ & \geq (r_1^T r_2 - r_{\min}^2) (r_1^T r_2 - r_{\min}^2). \end{aligned} \quad (26)$$

To prove (26), we consider the following two cases:

- (i)  $r_1^T r_2 - r_{\min}^2 \geq 0$  holds. Since  $t_{\min} \in (0, 1)$  holds in (24), it follows that  $r_1^T r_1 \geq r_1^T r_2$  and  $r_2^T r_2 \geq r_1^T r_2$ . Thus, we can obtain that

$$\begin{aligned} r_1^T r_1 - r_{\min}^2 & \geq r_1^T r_2 - r_{\min}^2 \geq 0, \\ r_2^T r_2 - r_{\min}^2 & \geq r_1^T r_2 - r_{\min}^2 \geq 0, \end{aligned}$$

which proves (26).

- (ii)  $r_1^T r_2 - r_{\min}^2 < 0$  holds. Without loss of generality, we can assume that  $r_1^T r_1 \leq r_2^T r_2$ . Then, it is easy to show that  $r_1^T r_1 \geq r_{\min}^2 + \frac{1}{4}\|l_2 - l_1\|_2^2$  given (22). It can be further combined with the simple fact that  $l_2 - l_1 = q_2 - q_1 - p_2 + p_1 = r_2 - r_1$ , which leads to

$$\begin{aligned} r_1^T r_1 & \geq r_{\min}^2 + \frac{1}{4}\|r_2 - r_1\|_2^2 \\ & = r_{\min}^2 + \frac{1}{4}(r_1^T r_1 + r_2^T r_2 - 2r_1^T r_2) \\ & \geq r_{\min}^2 + \frac{1}{4}(2r_1^T r_1 - 2r_1^T r_2). \end{aligned}$$

After re-organizing the terms, we have

$$r_2^T r_2 \geq r_1^T r_1 \geq 2r_{\min}^2 - r_1^T r_2,$$

and

$$\begin{aligned} r_1^T r_1 - r_{\min}^2 & \geq r_{\min}^2 - r_1^T r_2 \geq 0, \\ r_2^T r_2 - r_{\min}^2 & \geq r_{\min}^2 - r_1^T r_2 \geq 0. \end{aligned}$$

Similar to the previous case, it implies that (26) holds.

Now, the proof is completed.  $\blacksquare$

*Proof of Proposition 1:* For robots  $i$  and  $j$ , if  $p_k^i \in \mathcal{V}_k^{ij}$  and  $p_k^j \in \mathcal{V}_k^{ji}$  hold, it follows that  $a_k^{ijT} p_k^j \geq b_k^{ij}$  and  $a_k^{jiT} p_k^i \geq b_k^{ji}$ , respectively. Hence,  $a_k^{ijT} p_k^j + a_k^{jiT} p_k^i \geq b_k^{ij} + b_k^{ji}$  holds. Substituting (7) into it, the following holds:

$$a_k^{ijT} (p_k^i - p_k^j) \geq r'_{\min}.$$

Moreover, since  $a_k^{ijT} (p_k^i - p_k^j) \leq \|a_k^{ij}\|_2 \|p_k^i - p_k^j\|_2 \leq \|p_k^i - p_k^j\|_2$ , (8) can be easily derived.

For robot  $i$ , it clearly holds that  $p_{k-1}^i \in \mathcal{V}_{k-1}^{ij}$  and  $p_k^i \in \mathcal{V}_k^{ij}$ . The same applies to robot  $j$ . Due to (8), it can be shown that

$$\|p_{k-1}^i - p_{k-1}^j\|_2 \geq r'_{\min} = \sqrt{r_{\min}^2 + h^2 v_{\max}^2}$$

and

$$\|p_k^i - p_k^j\|_2 \geq r'_{\min} = \sqrt{r_{\min}^2 + h^2 v_{\max}^2}$$

hold. Then, during the time interval  $[t+kh-h, t+kh]$ , robot  $i$  moves from  $p_{k-1}^i$  to  $p_k^i$  at a constant velocity and robot  $j$  from  $p_{k-1}^j$  to  $p_k^j$ . If the minimum distance between robots  $i$  and  $j$  during  $[t+kh-h, t+kh]$  is larger than  $r_{\min}$ , then Proposition 1 holds.

Since the maximum allowable velocity is  $v_{\max}$ , it follows that  $\|p_k^i - p_{k-1}^i\|_2 \leq h v_{\max}$  and  $\|p_k^j - p_{k-1}^j\|_2 \leq h v_{\max}$ . Consequently, the following

$$\begin{aligned} \|p_k^i - p_k^j\|_2 &\geq \sqrt{r_{\min}^2 + h^2 v_{\max}^2} \\ &\geq \sqrt{r_{\min}^2 + \frac{1}{4} \left( \|p_k^i - p_{k-1}^i\|_2 + \|p_k^j - p_{k-1}^j\|_2 \right)^2} \\ &\geq \sqrt{r_{\min}^2 + \frac{1}{4} \|p_k^i - p_{k-1}^i - p_k^j + p_{k-1}^j\|_2^2} \end{aligned}$$

holds. Similarly, it holds that

$$\|p_{k-1}^i - p_{k-1}^j\|_2 \geq \sqrt{r_{\min}^2 + \frac{1}{4} \|p_{k-1}^i - p_{k-1}^j - p_k^i + p_{k-1}^j\|_2^2}.$$

Given these two conditions, it follows directly by Lemma 2 that

$$\|p_{k-1}^i + t(p_k^i - p_{k-1}^i) - p_{k-1}^j - t(p_k^j - p_{k-1}^j)\|_2 \geq r_{\min}.$$

That is, the minimum distance between robots  $i$  and  $j$  during the time interval  $[t + kh - h, t + kh]$  is larger than  $r_{\min}$ . This completes the proof.  $\blacksquare$

#### APPENDIX B PROOF OF LEMMA 1

*Proof:* To begin with, the constraint (2d) in the convex program (10) can be directly expanded as  $x_k^i = \mathbf{A}^k x_0^i + \mathbf{A}^{k-1} \mathbf{B} u_0^i + \dots + \mathbf{B} u_{k-1}^i$ . Moreover, the Lagrange function of (10) is given by

$$\begin{aligned} \mathcal{L}^i = & C^i + \sum_k^u \lambda_k^i (\|\Theta_a u_{k-1}^i\|_2 - u_{\max}) \\ & + \sum_k^v \lambda_k^i (\|\Theta_v v_k^i\|_2 - v_{\max}) \\ & + \sum_k \sum_{j \neq i} \lambda_k^{ij} (b_k^{ij} - a_k^{ijT} p_k^i) + t \nu^{iT} v_k^i \\ & + \sum_k \nu_k^{iT} (x_k^i - \mathbf{A}^k x_0^i - \mathbf{A}^{k-1} \mathbf{B} u_0^i - \dots - \mathbf{B} u_{k-1}^i), \end{aligned}$$

where  $^u \lambda_k^i$ ,  $^v \lambda_k^i$ ,  $\lambda_k^{ij}$ ,  $\nu_k^i = [{}^p \nu_k^{iT}, {}^v \nu_k^{iT}]^T$  and  ${}^t \nu^i$  are the Lagrangian multipliers corresponding to the inequality and equality constraints, where  $k = 1, 2, \dots, K$ .

When a deadlock happens, all robots remain static, i.e.,  $u_{k-1}^i = \mathbf{0}_d$  and  $v_k^i = \mathbf{0}_d$ . It implies that both  $\|\Theta_a u_{k-1}^i\|_2 < u_{\max}$  and  $\|v_k^i\|_2 < v_{\max}$  hold. Hence, according to the complementary slackness condition of Karush-Kuhn-Tucker (KKT) [44],  $^u \lambda_k^i = 0$  and  $^v \lambda_k^i = 0$  hold at the optimal solution of (10). Furthermore, according to the stationary condition of KKT, the following conditions are satisfied:

$$\frac{\partial \mathcal{L}^i}{\partial p_k^i} = \frac{\partial C^i}{\partial p_k^i} - \sum_{j \neq i} \lambda_k^{ij} a_k^{ij} + {}^p \nu_k^i = 0, \quad (27a)$$

$$\frac{\partial \mathcal{L}^i}{\partial v_k^i} = \begin{cases} {}^v \nu_k^i, & k \neq K \\ {}^v \nu_k^i + {}^t \nu^i, & k = K \end{cases} = 0, \quad (27b)$$

$$\begin{aligned} \frac{\partial \mathcal{L}^i}{\partial u_{k-1}^i} &= -\mathbf{B}^T \mathbf{A}^{T(K-k)} \nu_K^i - \mathbf{B}^T \mathbf{A}^{T(K-k-1)} \nu_{K-1}^i \\ &\quad - \dots - \mathbf{B}^T \nu_k^i = 0. \end{aligned} \quad (27c)$$

Given (3), it follows directly that

$$\mathbf{A}^m \mathbf{B} = \begin{bmatrix} m h \mathbf{I}_d \\ \mathbf{I}_d \end{bmatrix}. \quad (28)$$

Thus, condition (27c) can be re-formulated as

$${}^v \nu_K^{iT} \mathbf{A}^{K-k} \mathbf{B} + {}^v \nu_{K-1}^{iT} \mathbf{A}^{K-k-1} \mathbf{B} + \dots + {}^v \nu_k^{iT} \mathbf{B} = 0. \quad (29)$$

Furthermore, since  $\nu_K^{iT} \mathbf{B} = 0$ , it follows from (3) that  $[{}^p \nu_K^{iT}, {}^v \nu_K^{iT}]^T \begin{bmatrix} 0 \\ \mathbf{I}_d \end{bmatrix} = 0$ , which in turn implies  ${}^v \nu_K^i = 0$ . By condition (27b), it follows that  ${}^v \nu_k^i = 0$  holds,  $\forall k = 1, 2, \dots, K$ . Then (29) can be further simplified as

$$\begin{aligned} (K-k) h {}^p \nu_K^i + (K-k-1) h {}^p \nu_{K-1}^i \\ + \dots + h {}^p \nu_{k+1}^i = 0. \end{aligned}$$

By setting  $k = K - 1$ , it follows that  ${}^p \nu_K^i = 0$ . Hence, the other condition (27a) turns to

$$\frac{\partial \mathcal{L}^i}{\partial p_K^i} = \frac{\partial C^i}{\partial p_K^i} - \sum_{j \neq i} \lambda_K^{ij} a_K^{ij} = 0. \quad (30)$$

In addition, since  $p_K^i = p_{K-1}^i$  holds, the condition

$$\frac{\partial C^i}{\partial p_K^i} = Q_{\text{tar}} (p_K^i - p_{\text{target}}^i) + Q_{p|K-1} (p_K^i - p_{K-1}^i)$$

implies  $\frac{\partial C^i}{\partial p_K^i} = Q_{\text{tar}} (p_K^i - p_{\text{target}}^i)$ . In combination with (30), it follows that

$$Q_{\text{tar}} (p_{\text{target}}^i - p_K^i) + \sum_j \lambda_K^{ij} a_K^{ij} = 0,$$

where  $j \in \{j \in \mathcal{N} \mid \lambda_K^{ij} > 0\}$ . Since both robots  $i$  and  $j$  are at **Case 2** deadlock, the fact  $p^i(t) = p^i(t-h) = p_{K+1}^i(t-h) = \bar{p}_K^i(t)$  holds. In combination with (7), it can be derived that  $a_K^{ij} = \frac{p^i - p^j}{\|p^i - p^j\|_2}$ . This completes the proof.  $\blacksquare$

#### APPENDIX C PROOF OF EQUATION (15)

*Proof:* The Lagrange function of the new convex program is given by

$$\begin{aligned} \mathcal{L}^i = & C^i + \sum_{k=1}^K {}^u \lambda_k^i (\|\Theta_a u_{k-1}^i\|_2 - u_{\max}) \\ & + \sum_{k=1}^K {}^v \lambda_k^i (\|\Theta_v v_k^i\|_2 - v_{\max}) \\ & + \sum_{j \neq i} \lambda_k^{ij} (b_K^{ij} + w^{ij} - a_K^{ijT} p_K^i) + \sum_{j \neq i} w \lambda^{ij} (w^{ij} - \epsilon) \\ & + \sum_{k=1}^{K-1} \sum_{j \neq i} \lambda_k^{ij} (b_k^{ij} - a_k^{ijT} p_k^i) + t \nu^{iT} v_k^i \\ & + \sum_{k=1}^K \nu_k^{iT} (x_k^i - \mathbf{A}^k x_0^i - \mathbf{A}^{k-1} \mathbf{B} u_0^i - \dots - \mathbf{B} u_{k-1}^i), \end{aligned}$$

where  ${}^w \lambda^{ij}$  are the Lagrangian multipliers corresponding to the inequality constraints. Similar to the proof of Lemma 1, it

follows that  ${}^u\lambda_k^i = 0$  and  ${}^v\lambda_k^i = 0$ . Additionally, by the KKT condition, the following conditions:

$$\frac{\partial \mathcal{L}^i}{\partial p_K^i} = \frac{\partial C^i}{p_K^i} - \sum_{j \neq i} \lambda_K^{ij} a_K^{ij} + p_{\nu_K^i} = 0, \quad (31a)$$

$$\frac{\partial \mathcal{L}^i}{\partial w^{ij}} = \frac{\partial C^i}{\partial w^{ij}} + \lambda_K^{ij} + {}^w\lambda^{ij} = 0, \quad (31b)$$

hold. Thus, it can be similarly derived that both  ${}^p\nu_K^i = 0$  and

$$\frac{\partial \mathcal{L}^i}{\partial p_K^i} = \frac{\partial C^i}{p_K^i} - \sum_{j \neq i} \lambda_K^{ij} a_K^{ij} = 0.$$

To proceed further, the following fact:

$${}^w\lambda^{ij} = 0, \forall j \neq i \quad (32)$$

will be proven by contradiction. By substituting (9) into (31b), it follows that

$$\rho_0 \left( -\frac{1}{w^{ij}} + \frac{1}{\epsilon} \right) + \lambda_K^{ij} + {}^w\lambda^{ij} = 0. \quad (33)$$

If  ${}^w\lambda^{ij} > 0$  holds, due to the complementary slackness condition of KKT, then  $w^{ij} = \epsilon$  holds. Thus, the above equation implies  $\lambda_K^{ij} + {}^w\lambda^{ij} = 0$ . However, the KKT condition implies that both  ${}^w\lambda^{ij} \geq 0$  and  $\lambda_K^{ij} \geq 0$  must hold. Thus,  ${}^w\lambda^{ij} = 0, \forall j \neq i$ .

Therefore, via (13), (31b) and (32), it follows that

$$\lambda_K^{ij} = -\frac{\partial C^i}{\partial w^{ij}} = -\rho_0 \frac{w^{ij} - \epsilon}{\epsilon w^{ij}}. \quad (34)$$

By substituting (34) into (31a), it can be derived that

$$Q_{\text{tar}} (p_{\text{target}}^i - p_K^i) + \sum_{j \neq i} a_K^{ij} \rho_0 \frac{\epsilon - w^{ij}}{\epsilon w^{ij}} = 0.$$

Lastly, if  $j \notin \mathbb{A}^i$ , then both  $w^{ij} = \epsilon$  and  $\frac{w^{ij} - \epsilon}{\epsilon w^{ij}} = 0$  hold, which implies (15).

Next, it remains to be shown that  $w^{ij} = w^{ji}$  holds. If  $w^{ij} < \epsilon$ , it clearly follows that  $\rho_0 \left( -\frac{1}{w^{ij}} + \frac{1}{\epsilon} \right) < 0$  and  $\lambda_K^{ij} > 0$  by the conditions in (32) and (33). This implies that the constraint (14b) is active, i.e.,

$$a_K^{ijT} p_K^i = b_K^{ij} + w^{ij}. \quad (35)$$

Note that  $p_K^i(t) = p^i(t) = p^i(t-h) = p_K^i(t-h) = p_{K+1}^i(t-h) = \bar{p}_K^i(t)$  holds for robot  $i$  and similar condition holds for robot  $j$ . Hence, by (7) and (35), it follows that

$$\frac{\|p_K^i - p_K^j\|_2}{2} = \frac{r'_{\min}}{2} + w^{ij}.$$

Similarly, for robot  $j$ , it can be derived that

$$\frac{\|p_K^j - p_K^i\|_2}{2} = \frac{r'_{\min}}{2} + w^{ji}.$$

Consequently, these two equations imply that  $w^{ij} = w^{ji}$ . This completes the proof. ■

## REFERENCES

- [1] S.-J. Chung, A. A. Paranjape, P. Dames, S. Shen, and V. Kumar, "A survey on aerial swarm robotics," *IEEE Transactions on Robotics*, vol. 34, no. 4, pp. 837–855, 2018.
- [2] S. Huang, R. S. H. Teo, and K. K. Tan, "Collision avoidance of multi unmanned aerial vehicles: A review," *Annual Reviews in Control*, vol. 48, pp. 147–164, 2019.
- [3] J. Borenstein and Y. Koren, "Real-time obstacle avoidance for fast mobile robots," *IEEE Transactions on systems, Man, and Cybernetics*, vol. 19, no. 5, pp. 1179–1187, 1989.
- [4] —, "The vector field histogram-fast obstacle avoidance for mobile robots," *IEEE Transactions on Robotics and Automation*, vol. 7, no. 3, pp. 278–288, 1991.
- [5] Y. Koren and J. Borenstein, "Potential field methods and their inherent limitations for mobile robot navigation," in *IEEE International Conference on Robotics and Automation*, vol. 2, 1991, pp. 1398–1404.
- [6] P. Fiorini and Z. Shiller, "Motion planning in dynamic environments using velocity obstacles," *International Journal of Robotics Research*, vol. 17, no. 7, pp. 760–772, 1998.
- [7] J. Alonso-Mora, A. Breitenmoser, P. Beardsley, and R. Siegwart, "Reciprocal collision avoidance for multiple car-like robots," in *2012 IEEE International Conference on Robotics and Automation*, 2012, pp. 360–366.
- [8] J. van den Berg, M. Lin, and D. Manocha, "Reciprocal velocity obstacles for real-time multi-agent navigation," in *2008 IEEE International Conference on Robotics and Automation*, 2008, pp. 1928–1935.
- [9] J. van den Berg, S. J. Guy, M. Lin, and D. Manocha, "Reciprocal n-body collision avoidance," in *14th International Symposium on Robotics Research (ISSR)*, vol. 70, 2011, pp. 3–19.
- [10] K. Cole and A. M. Wickenheiser, "Reactive trajectory generation for multiple vehicles in unknown environments with wind disturbances," *IEEE Transactions on Robotics*, vol. 34, no. 5, pp. 1333–1348, 2018.
- [11] L. Pallottino, V. G. Scordio, A. Bicchi, and E. Frazzoli, "Decentralized cooperative policy for conflict resolution in multivehicle systems," *IEEE Transactions on Robotics*, vol. 23, no. 6, pp. 1170–1183, 2007.
- [12] C. Tomlin, G. Pappas, and S. Sastry, "Conflict resolution for air traffic management: a study in multiagent hybrid systems," *IEEE Transactions on Automatic Control*, vol. 43, no. 4, pp. 509–521, 1998.
- [13] B. Rivière, W. Hönig, Y. Yue, and S.-J. Chung, "Glas: Global-to-local safe autonomy synthesis for multi-robot motion planning with end-to-end learning," *IEEE Robotics and Automation Letters*, vol. 5, no. 3, pp. 4249–4256, 2020.
- [14] T. Fan, P. Long, W. Liu, and J. Pan, "Distributed multi-robot collision avoidance via deep reinforcement learning for navigation in complex scenarios," *International Journal of Robotics Research*, vol. 39, no. 7, pp. 856–892, 2020.
- [15] G. Shi, W. Hönig, X. Shi, Y. Yue, and S.-J. Chung, "Neural-swarm2: Planning and control of heterogeneous multirobot swarms using learned interactions," *IEEE Transactions on Robotics*, pp. 1–17, 2021.
- [16] Y. F. Chen, M. Liu, M. Everett, and J. P. How, "Decentralized non-communicating multiagent collision avoidance with deep reinforcement learning," in *2017 IEEE International Conference on Robotics and Automation (ICRA)*, 2017, pp. 285–292.
- [17] D. Ioan, I. Prodan, S. Olaru, F. Stoican, and S.-I. Niculescu, "Mixed-integer programming in motion planning," *Annual Reviews in Control*, 2020.
- [18] A. Richards and J. How, "Decentralized model predictive control of cooperating uavs," in *43rd IEEE Conference on Decision and Control*, 2004, pp. 4286–4291.
- [19] D. R. Robinson, R. T. Mar, K. Estabridis, and G. Hewer, "An efficient algorithm for optimal trajectory generation for heterogeneous multi-agent systems in non-convex environments," *IEEE Robotics and Automation Letters*, vol. 3, no. 2, pp. 1215–1222, 2018.
- [20] S. Tang, J. Thomas, and V. Kumar, "Hold or take optimal plan (hoop): A quadratic programming approach to multi-robot trajectory generation," *International Journal of Robotics Research*, vol. 37, no. 9, pp. 1062–1084, 2018.
- [21] J. Yu and S. M. LaValle, "Optimal multirobot path planning on graphs: Complete algorithms and effective heuristics," *IEEE Transactions on Robotics*, vol. 32, no. 5, pp. 1163–1177, 2016.
- [22] F. Augugliaro, A. P. Schoellig, and R. D'Andrea, "Generation of collision-free trajectories for a quadcopter fleet: A sequential convex programming approach," in *2012 IEEE/RSJ International Conference on Intelligent Robots and Systems*, 2012, pp. 1917–1922.

- [23] D. Morgan, G. P. Subramanian, S.-J. Chung, and F. Y. Hadaegh, "Swarm assignment and trajectory optimization using variable-swarm, distributed auction assignment and sequential convex programming," *International Journal of Robotics Research*, vol. 35, no. 10, pp. 1261–1285, 2016.
- [24] Y. Chen, M. Cutler, and J. P. How, "Decoupled multiagent path planning via incremental sequential convex programming," in *2015 IEEE International Conference on Robotics and Automation (ICRA)*, 2015, pp. 5954–5961.
- [25] L. C. E. and A. P. Schoellig, "Trajectory generation for multiagent point-to-point transitions via distributed model predictive control," *IEEE Robotics and Automation Letters*, vol. 4, no. 2, pp. 375–382, 2019.
- [26] L. Wang, A. D. Ames, and M. Egerstedt, "Safety barrier certificates for collisions-free multirobot systems," *IEEE Transactions on Robotics*, vol. 33, no. 3, pp. 661–674, 2017.
- [27] J. Park and H. J. Kim, "Online trajectory planning for multiple quadrotors in dynamic environments using relative safe flight corridor," *IEEE Robotics and Automation Letters*, vol. 6, no. 2, pp. 659–666, 2021.
- [28] W. Hönig, J. A. Preiss, T. K. S. Kumar, G. S. Sukhatme, and N. Anayan, "Trajectory planning for quadrotor swarms," *IEEE Transactions on Robotics*, vol. 34, no. 4, pp. 856–869, 2018.
- [29] L. Campos-Macias, D. Gomez-Gutierrez, R. Aldana-Lopez, R. de la Guardia, and J. I. Parra-Vilchis, "A hybrid method for online trajectory planning of mobile robots in cluttered environments," *IEEE Robotics and Automation Letters*, vol. 2, no. 2, pp. 935–942, 2017.
- [30] P. Wang and B. Ding, "A synthesis approach of distributed model predictive control for homogeneous multi-agent system with collision avoidance," *International Journal of Control*, vol. 87, no. 1, pp. 52–63, 2014.
- [31] D. Zhou, Z. Wang, S. Bandyopadhyay, and M. Schwager, "Fast, on-line collision avoidance for dynamic vehicles using buffered Voronoi cells," *IEEE Robotics and Automation Letters*, vol. 2, no. 2, pp. 1047–1054, 2017.
- [32] R. A. Knepper and D. Rus, "Pedestrian-inspired sampling-based multi-robot collision avoidance," in *2012 IEEE RO-MAN: The 21st IEEE International Symposium on Robot and Human Interactive Communication*, 2012, pp. 94–100.
- [33] J. Alonso-Mora, J. A. DeCastro, V. Raman, D. Rus, and H. Kress-Gazit, "Reactive mission and motion planning with deadlock resolution avoiding dynamic obstacles," *Autonomous Robots*, vol. 42, no. 4, pp. 801–824, 2018.
- [34] J. S. Grover, C. Liu, and K. Sycara, "Deadlock analysis and resolution for multi-robot systems," in *International Workshop on the Algorithmic Foundations of Robotics*. Springer, 2020, pp. 294–312.
- [35] J. Tordesillas and J. P. How, "Mader: Trajectory planner in multiagent and dynamic environments," *IEEE Transactions on Robotics*, pp. 1–14, 2021.
- [36] J. Alonso-Mora, P. Beardsley, and R. Siegwart, "Cooperative collision avoidance for nonholonomic robots," *IEEE Transactions on Robotics*, vol. 34, no. 2, pp. 404–420, 2018.
- [37] U. Eren, A. Prach, B. B. Kocer, S. V. Rakovic, E. Kayacan, and B. Acikmese, "Model predictive control in aerospace systems: Current state and opportunities," *Journal of Guidance Control and Dynamics*, vol. 40, no. 7, pp. 1541–1566, 2017.
- [38] S. Liu, M. Watterson, K. Mohta, K. Sun, S. Bhattacharya, C. J. Taylor, and V. Kumar, "Planning dynamically feasible trajectories for quadrotors using safe flight corridors in 3-D complex environments," *IEEE Robotics and Automation Letters*, vol. 2, no. 3, pp. 1688–1695, 2017.
- [39] K. Nagel, D. E. Wolf, P. Wagner, and P. Simon, "Two-lane traffic rules for cellular automata: A systematic approach," *Physical Review E*, vol. 58, no. 2, pp. 1425–1437, 1998.
- [40] S. Diamond and S. Boyd, "CVXPY: A Python-embedded modeling language for convex optimization," *Journal of Machine Learning Research*, vol. 17, no. 83, pp. 1–5, 2016.
- [41] E. D. Andersen and K. D. Andersen, *The Mosek Interior Point Optimizer for Linear Programming: An Implementation of the Homogeneous Algorithm*. Boston, MA: Springer US, 2000, pp. 197–232.
- [42] L. C. E., "Multiagent planning," Website, [https://github.com/carlosluis/multiagent\\_planning](https://github.com/carlosluis/multiagent_planning).
- [43] D. Mellinger and V. Kumar, "Minimum snap trajectory generation and control for quadrotors," in *2011 IEEE International Conference on Robotics and Automation*, 2011, pp. 2520–2525.
- [44] S. Boyd, S. P. Boyd, and L. Vandenberghe, *Convex Optimization*. Cambridge University Press, 2004.